Sl. No.	IIT Ropar List of Recent Publications with Abstract Coverage: September, 2026
A	**Book Chapter(s)**
1.	Bandgap reference circuits for AI hardware: Challenges, design trade-offs, and optimization strategies **MK Singh**, R Nagulapalli, **DM Das, M Sakare** - VLSI Design for Artificial Intelligence and Machine Learning Applications: Book Chapter, 2026 **Abstract:** Bandgap reference (BGR) circuits play a critical role in ensuring power stability and precision in modern artificial intelligence (AI) hardware, including Tensor Processing Units, Neural Processing Units, and Graphics Processing Units. However, as semiconductor technology scales to sub-7-nm FinFET and gate-all-around transistors, process variations and device mismatches introduce random voltage offsets, which can degrade model accuracy, power efficiency, and computational reliability in deep learning accelerators. To mitigate these challenges, advanced layout techniques such as common-centroid transistor placement, matched resistor arrays, and dummy structures are employed, along with digital trimming, adaptive biasing, and curvature compensation, to enhance voltage accuracy and thermal stability. Furthermore, designing BGR circuits for AI applications involves a trade-off between area, accuracy, and power dissipation. High-precision BGR circuits with low-temperature coefficient designs improve voltage stability but increase circuit complexity and power consumption, making them unsuitable for battery-operated edge AI and Internet of Things devices. Conversely, low-power BGR circuits, optimized for wearables, smart sensors, and edge computing, focus on minimal leakage currents and efficient biasing techniques, sometimes at the cost of accuracy and robustness against supply variations. However, high-performance AI accelerators in cloud data centers require ultra-low drift and high-stability BGR circuits, often consuming additional silicon area due to compensation circuits. This chapter explores the challenges of design trade-offs in AI-focused BGR circuits, highlighting strategies for designing and optimizing power efficiency and computational reliability in emerging AI architectures. This chapter provides a detailed analysis of the BGR circuits for AI and machine learning applications, offering a comprehensive understanding of the topic. It also compares
2.	Brain signal processing with a focus on electroencephalography in attention-deficit hyperactivity disorder **G Gangwar**, N Singh…SL Tripathi - Brain-to-Computer Interfaces Using Machine Learning and Deep Learning: Book Chapter, 2026 **Abstract:** In recent days, machine learning has become an effective method to automatically detect patterns in data, which can be used to predict future data for better decisions at times of uncertainty. This chapter describes the wide range of applications and methodologies utilized in brain signal processing, concentrating on electroencephalography (EEG) in attention-deficit hyperactivity disorder (ADHD) patients. It becomes an effective instrument for decoding brain signals, simplifying the extraction of significant patterns from intricate neural data. We examine fundamental machine learning paradigms, such as supervised and unsupervised, and their significance in interpreting cognitive states, motor intentions, and neurological disorders. After that, we discussed feature extraction techniques, including time-frequency analysis and wavelet transforms. Autoencoders and reptile search algorithms are examined to improve signal representation. This study proposes random forest classifiers for distinguishing ADHD individuals from non-ADHD ones and other standard classifiers used to compare model performance, such as

	XGBoost, SVMs, k-nearest neighbors, and AdaBoost. Classifiers are also evaluated for their performance in decoding cognitive and motor intentions and for handling the spatiotemporal intricacies of brain signals. The proposed model provided an accuracy of 92%, the same value achieved for recall, precision, and F1 score, as well as a specificity rate of 92% and a sensitivity rate of 92%. Apart from this, the ROC_AUC score of 0.92 was achieved for this model, which shows that the random forest has an improved capability to distinguish between ADHD and non-ADHD individuals.
3.	High-speed continuous-time linear equalizers for ai and machine learning hardware: Design, optimization, and linearity enhancement **P Singh, R Walia, R Nagulapalli, M Sakare** - VLSI Design for Artificial Intelligence and Machine Learning Applications: Book Chapter, 2026 **Abstract:** The rapid advancements in artificial intelligence (AI) and machine learning (ML) have resulted in a significant increase in data transfer rates, requiring high-speed and energy-efficient communication systems. In high-speed wire line and optical links, signal degradation due to channel loss and inter-symbol interference (ISI) poses a significant challenge, impacting system performance and accuracy. Continuous time linear equalizers (CTLEs) are crucial in compensating for these distortions, enabling reliable high-speed data transmission for artificial intelligence (AI) and machine learning (ML) hardware. The continuous-Time Linear Equalizers (CTLEs) are essential in high-speed VLSI serial link receivers to counteract frequency-dependent channel attenuation and eliminate Inter-Symbol Interference (ISI). Unlike digital equalizers (like Feed Forward Equalizers), analog CTLEs operate without a clock signal. This minimizes power consumption and saves chip area, making them highly efficient for receivers. This chapter focuses on the design, optimization, and linearity enhancement of high-speed continuous time linear equalizers (CTLEs) to meet the stringent requirements of artificial intelligence (AI) and machine learning (ML) systems. Linearity-improved continuous time linear equalizers (CTLEs) architecture enhances circuit linearity by replacing traditional current sources with high-linearity poly resistors. The core innovation of this design is the implementation of a voltage-to-current (V2I) converter in place of the conventional current source within the continuous time linear equalizers (CTLEs) biasing circuitry. The primary advantage of this innovative modification is a substantial improvement in the circuit's linearity, resulting in a notable reduction in total harmonic distortion (THD). The standard 65-nm complementary metal-oxide-semiconductor (CMOS) technology and a 1-V power supply were used to design and implement the continuous time linear equalizers (CTLEs). The overall active area occupied by the circuit is 0.023 mm^2, demonstrating an efficient and compact layout suitable for modern high speed transceiver applications. The performance evaluations indicate that the continuous time linear equalizers (CTLEs) delivers superior signal equalization when applied to a 12-inch transmission channel at a data rate of 12.5 Gb/s. The simulation results reveal an eye width of 71.24 ps and an eye height of 98.82 mV, ensuring a clear and distinguishable data signal. The measured jitter is also 8.63 ps, further validating the circuit's ability to maintain signal integrity and reduce timing uncertainty. In terms of power efficiency, the linearity-improved continuous time linear equalizers (CTLEs) consume only 3.29 mW, achieving a figure of merit (FoM) of 0.26 pJ/b. These advancements represent a significant step forward in developing high-performance continuous time linear equalizers (CTLEs) circuits.
4.	Recent developments in modelling strategies of laser powder bed fusion **R Kumar,** SK Nandi, **A Agrawal** - Additive Manufacturing: Book Chapter, 2026 **Abstract:** Modelling of laser powder bed fusion (LPBF)-based additive manufacturing process garners considerable attention from researchers and industry professionals to develop

	predictive simulation models to capture the intricate multiphysics phenomenon. Melt pool dynamics directly influence the microstructure and consequently the mechanical response of the components fabricated by LPBF. The mathematical formulations and their solving strategies across different time and length scales are essential for the fundamental understanding of spatial and temporal temperature distributions. The primary objective of this chapter is to explore and present the recent progress in the computing methods concerned with melt pool modelling. Mesh-based numerical approaches, such as Finite Element Method (FEM) and Finite Volume Method (FVM), to solve Computational Fluid Dynamics (CFD) algorithms for domains discretised into nodes and control volumes, respectively, are well-established in generating high-fidelity solutions for fluid flow modelling in melt pools. Recent advancements in the thermal modelling of LPBF include the particle modelling-based Lattice Boltzmann approach and mesh-free Smooth Particle Hydrodynamics (SPH), which can accommodate multiple materials, complex interphase boundaries, and the dynamics of free surfaces. To curb the computational cost involved in the aforementioned techniques, semi-analytical methods have evolved to simplify the solving framework of complex mathematical functions. Alongside physics-based modelling, data-driven artificial neural network (ANN) surrogate models are being established to predict the real-time evolution of temperature and density in laser-based additive manufacturing.
5.	Thermal pyrolysis of plastic waste into fuel **T Mondal** - 2026 - Sustainable Plastic Waste Management, Volume 2: Book Chapter, 2026 **Abstract:** Recently, tackling with the twin problem of energy conversion and environmental protection has gained the attention of researchers globally. One of the most attractive alternate solutions to these problems is pyrolysis of plastic waste into useful fuels (gas and diesel). It is an efficient waste management technique for converting plastic waste into energy and thereby contributing in the development of a sustainable alternative to the fossil fuels to meet the increasing energy demand. This chapter enlightens the prospect and significance of the thermal pyrolysis of plastic waste into fuel oil.
B	**Conference Proceeding(s)**
6.	A dual-function switchable RIS unit cell for reflection and energy harvesting at a single frequency **P Rattanpal, S Bansal, A Sharma** - 2026 IEEE International Symposium on Antennas and Propagation and USNC-URSI Radio Science Meeting (AP-S/USNC-URSI), 2026 **Abstract:** A dual-functional reconfigurable intelligent surface (RIS) unit cell is proposed for sub-6 GHz operation that supports both reflective beam steering and energy harvesting (EH) modes. A single PIN diode (P1) is used to control the reflection phase in communication mode, enabling 1-bit phase modulation. Another PIN diode (P2) is used to select the mode of operation between EH and communication of the unit cell. In the P2 OFF state, the unit cell is reconfigured to redirect incident RF energy to a passive rectifying load. The rectifier is placed at an optimized location to maximize power transfer and converts the incident RF into DC power. This DC power can be utilized to recharge the RIS controller's energy storage. In this work, a common operating frequency of 5.6 GHz is employed for both modes. The proposed unit cell is validated through full-wave simulations, demonstrating clear separation between EH and communication functionality. This design, hence, enables switchable RIS deployment with minimal switching complexity.

7.	A novel low-computation parameter identification method for lithium-ion cells **P Kannojia, A Ahmad, AVR Teja** - 2026 IEEE 6th International Conference on Sustainable Energy and Future Electric Transportation (SEFET), 2026 **Abstract:** This paper presents a fast parameter identification method with low-complexity for the first-order Thevenin equivalent circuit model of Lithium-ion cells using a series of voltage and current excitation tests. The proposed technique employs short-duration voltage and current excitations to sequentially estimate the open circuit voltage VOCV, ohmic resistance R0, polarization capacitance C1 and polarization resistance R1 by simplifying the equivalent circuit into reduced-order representation. The proposed method neither requires OCV-SoC data nor voltage-current test data stored offline to be analyzed later with complex mathematical calculations. This significantly reduces computational burden and memory usage. The proposed method is implemented in simulation using MATLAB/Simulink software and the results are provided over a wide range of state-of-charge (SoC) levels. The results demonstrate a high estimation accuracy within a maximum parameter identification error of 5% at all SoCs.
8.	Advancing multimodal fusion on heterogeneous medical data with hybrid geometry attention **J Dhar**, MK Pandey…F Sohel, **P Goyal** - Proceedings of the 32nd ACM SIGKDD Conference on Knowledge Discovery and Data Mining V.2, 2026 **Abstract:** Multimodal fusion learning (MFL) (a framework to jointly learn from heterogeneous data sources) has shown great potential in various fields such as Medicine, Science, and Engineering. It is extremely desirable in the medical domain, where we are faced with disparate data modalities such as imaging, clinical records, and omics. However, existing MFL strategies face several major challenges. First, they struggle to capture complex cross-modal interactions effectively, which in turn limits performance improvements. Second, they incur high computational costs, restricting their applicability in resource-constrained healthcare AI applications. Finally, they are often designed and evaluated for narrow, fixed modality configurations (e.g., imaging-only, or specific pairs such as image and omics), which limits evidence of their adaptability and generalizability to broader collections of heterogeneous medical modalities. To address these challenges, we propose a novel MFL framework – Cascaded Unified Representation Learning for Efficient Fusion Network (CURE) – a lightweight and scalable framework that progressively integrates various modalities through a novel efficient Hybrid Geometry Aware Fusion layer (HyFuse), where each HyFuse layer is sequentially learned for each modality, making the framework adaptable and generalizable. Within HyFuse, an efficient residual convolution module captures rich multi-scale features to ensure cost-effective learning, while a hybrid-space aware attention mixer learns coarse-to-fine structural cues to better preserve cross-modal relationships. Complementary learnable late-fusion and shared-information refinement modules are then employed to learn robust, modality-order-invariant shared features, which in turn yields consistent performance improvements. Extensive evaluations on 16 public datasets show that CURE outperforms leading multimodal fusion methods (e.g., DRIFA-Net and HEALNet), boosting performance by up to ≈ 3.97% and lowering computational costs by up to ≈ 87.8%, ensuring more effective and reliable predictions.
9.	Automated thermal imaging system for fault fuse detection: Enhancing electrical safety through intelligent infrared image analysis **N Rishik, CC Reddy** - 2026 IEEE Guwahati Subsection Conference (GCON), 2026 **Abstract:** Proper detection of any thermal anomalies in the systems of electrical fuses is critical in the operation and safety of the fuse, as well as the reduction of delays in maintenance. The paper provides a data driven system of automated monitoring of fuse conditions based on an infrared

	thermal imaging system and deep learning. The suggested system is based on a two step pipeline with the thermal images being analyzed by a convolutional neural network to detect the conditions of the fuses as normal, overheated, or missing. With the fuse being declared to be normal, then the system explicitly verifies that everything is functioning correctly; otherwise, during overheating or with a lost fuse, a special localization phase is triggered to know the exact location of the fault in the panel. This is done by a grid based spatial segmentation approach, whereby detected thermal anomalies are mapped to their physical fuse locations, allowing clear and understandable diagnostics. As an augmentation to strengthening, temperature based filtering is added to imprecise the detection of anomalies in different conditions. It is trained and tested on a curated dataset that has a variety of fuse states reaching an accuracy of over 94% in classifying as well as localizing with an average Intersection over Union (IoU) of 0.88. The proposed solution offers an efficient, scalable, and non contact alternative to traditional inspection solutions that can substantially decrease the amount of manual labor required and increase reliability and allow timely maintenance in current electrical systems.
10.	Cut, stitch, adapt: Data-efficient and low-calibration speech BCIs **A Naskar, A Naskar, D Bathula** - International Conference on Medical Image Computing and Computer-Assisted Intervention (MICCAI-2026), 2026 **Abstract:** Intracortical Brain–Computer Interfaces (iBCIs) for speech decoding show immense promise in translating neural activity into text. However, clinical viability remains severely constrained by labeled data scarcity and the continuous physical drift of neural representations over time. Contemporary approaches increasingly rely on massive cross-species pretraining and large ensembles, incurring prohibitive costs while still requiring daily recalibration to counteract electrode drift. We propose a data-efficient pipeline that requires only 40 hrs of patient data and achieves domain generalization to unseen recording sessions. To overcome data limitations, we propose Neural Cut-and-Stitch (NCS), a signal-space augmentation strategy. By isolating word-level neural patterns from past recordings, we apply crossfade stitching to synthesize brain signals for entirely new sentences. We also introduce an Adversarial Domain Adaptation (ADAN) framework to improve generalization to unseen sessions. This explicitly enforces a session-invariant neural manifold, retaining acoustic decoding performance with far lesser calibration. Experiments on the Brain-to-Text ’25 benchmark demonstrate that NCS alone reduces the Phoneme Error Rate (PER) from 10.1% to 8.8% on the held-out test set. Combining it with the baseline, we reduce the Word Error Rate (WER) from 7.0% to 4.8%. Concurrently, ADAN confines PER degradation on unseen sessions 15 d into the future to < 2% change. These gains show that signal augmentation and domain adaptation can be complementary to large-scale pretraining and reduce reliance on daily recalibration for deployment.
11.	Design and analysis of a general SHM technique for a 5-level CHB MLI with practical DC sources **A Dhiman, P Kalkal, AVR Teja** - 2026 IEEE 6th International Conference on Sustainable Energy and Future Electric Transportation (SEFET), 2026 **Abstract:** The analysis of CHB MLI for Selective Harmonic Elimination (SHE) or Selective Harmonic Mitigation (SHM) includes the effect of variation of the DC sources of different cells cascaded to achieve a desired n-level output phase voltage. If we consider cascading cells in the case of CHB MLI, it is not always possible to maintain the cell voltages at exactly the same voltage. Hence, if we use the same old solution (switching angles) as used for the cells with exactly the same voltage, we can notice a significant deviation in output Line to Line RMS fundamental voltage. Additionally, the harmonics of interest to be mitigated may also not be achieved. So, it is necessary to analyze the CHB MLI with varying, or practical, DC voltages. This paper proposes a

	simple yet robust technique for Selective Harmonic Mitigation with close to stiff Fundamental Line Voltage in case of 5-Level CHB MLI with varying(practical) DC Sources.
12.	Force-feedback RL-based bionic control of hand exoskeleton for object grasping and slip prevention **A Singh**…N Sarmah, SM Hazarika - 2026 IEEE Guwahati Subsection Conference (GCON), 2026 **Abstract:** This paper presents a force-feedback reinforcement learning (RL) based bionic control framework for a hand exoskeleton aimed at stable object grasping and slip prevention. A custom Unified Robot Description Format (URDF) model of the exoskeleton is developed and deployed in the PyBullet physics engine, with bio-mechanically motivated kinematic constraints implemented to capture realistic inter-joint coupling and finger synergies. To guide policy learning, a reward function is designed that explicitly incorporates fingertip force feedback and slip indicators, encouraging stable grasp formation while penalizing excessive contact forces and object loss. Slip-aware perception is achieved by integrating Haar wavelet–based features of force signals into the observation space, enabling early detection of transient contact disturbances.To improve robustness and sim-to-real transferability, domain randomization is applied during training by varying object mass, friction coefficient, and contact stiffness. The proposed controller is evaluated by comparing nominal and domain-randomized training regimes. Results demonstrate that the domain-randomized agent converges to higher average rewards and exhibits superior resistance to external disturbances. The findings validate the effectiveness of combining physics-aware modeling, wavelet-based slip perception, and domain-randomized reinforcement learning for robust bionic grasp control in hand exoskeleton systems.
13.	Frequency-based coherent area identification under disturbance conditions using PMU measurement and wavelet coherency application **A Kumar, BP Padhy** - 2026 IEEE 6th International Conference on Sustainable Energy and Future Electric Transportation (SEFET), 2026 **Abstract:** Identifying coherent areas during power system disturbances is crucial for wide-area monitoring, protection, and system stability. During events such as sudden load changes, line tripping and faults, phasor measurement unit (PMU)–based frequency measurements exhibit non-stationary and transient oscillatory behavior due to the excitation of electromechanical dynamics, which challenges conventional coherency identification methods. This paper proposed a PMU measurement–based method for identifying coherent areas under disturbance conditions using wavelet analysis of frequency signals, and a numerical wavelet coherency index is employed to quantify the dynamic coupling between different buses and to form coherent areas without relying on system model information or prior knowledge of disturbance location. The effectiveness of the proposed approach is validated using the Kundur two-area system and the IEEE 39-bus test system. Time-domain simulations and wavelet-based analyses are carried out in DIgSILENT PowerFactory and MATLAB. The results demonstrate that the proposed method reliably captures disturbance-induced coherency patterns and provides consistent area identification under non-stationary ring-down conditions.
14.	Harmonic elimination at point of common coupling (PCC) with switching angle correction in cascaded H-bridge multilevel inverters **S Kumar, AVR Teja** - 2026 IEEE 6th International Conference on Sustainable Energy and Future Electric Transportation (SEFET), 2026 **Abstract:** Multilevel inverters eliminate harmonics at the inverter terminals. These harmonics are also eliminated at the point of common coupling (PCC) if all the loads connected at PCC are linear. However, with nonlinear loads, though the harmonic is eliminated at the inverter terminals, it will

	re-appear at PCC due to the nonlinear currents drawn through the filter connected between the inverter and PCC. In this paper, a method is proposed to modify the switching angles of the multilevel inverter using which the harmonic content at PCC can be controlled/eliminated. The proposed method is theoretically verified and also tested in simulation using MATLAB/Simulink software and the results are reported. It is shown that the desired harmonic can be eliminated at PCC while supplying nonlinear loads just be modifying the switching angles without the need of any additional filters.
15.	Prompt and probe: Data-efficient adaptation of black-box foundation models via unified active visual prompting D Mahapatra…**J Dhar**, N Zaidi… - International Conference on Medical Image Computing and Computer-Assisted Intervention (MICCAI- 2026), 2026 **Abstract:** Deploying foundation models (FMs) in clinical imaging is limited by expert annotation cost and the opacity of API-served models that preclude gradient-based adaptation. Existing methods address these constraints separately: black-box prompt tuning assumes fixed labels, while active learning often requires gradients, internal features, logits, or calibrated probabilities. We present Prompt and Probe (P), a query-only framework for adapting frozen FMs to classification and segmentation while selecting informative unlabeled samples. A lightweight Visual Prompt Decoder (VIPD) maps shared semantic and anatomical embeddings to input-space prompts: global additive prompts for classification and spatial channel-concatenated prompts for segmentation, trained via zeroth-order optimization. For acquisition, the trained decoder probes unlabeled images with multi-scale perturbations; prompt and prediction shifts are summarized as image- and pixel-level instability scores and fused after per-batch normalization. Across seven public datasets, eight benchmarks, and six clinical modalities, P reduces labeling by 40– while outperforming black-box active learning baselines, achieving AUROC on CheXpert with labels and Dice on Kvasir-Seg with labels. Boundary instability from model-predicted masks, without segmentation ground truth, improves classification acquisition by up to 24.5 AUROC points, suggesting that joint spatial–semantic probing identifies anatomically ambiguous samples missed by task-specific selection.
16.	Proximity-constrained counterfactual decoding for hallucination-robust medical VQA D Mahapatra…**J Dhar**…I Razzak - European Conference on Computer Vision, 2026 **Abstract:** Hallucinations in medical vision language models arise when language priors override subtle visual evidence during decoding. Existing training-free contrastive decoding methods suppress these priors by contrasting logits against a globally perturbed image, but global perturbations destroy the very diagnostic cues they are meant to protect—standard VCD blur flips nearly one in five CheXpert labels on held-out chest radiographs. We propose Proximity-Constrained Counterfactual Decoding (PCCD), which admits a counterfactual view only when it satisfies both a global and an object-masked feature-space similarity bound, constraining diagnostic drift while increasing the contrastive margin for visually grounded tokens to first order under explicitly stated assumptions. Two complementary branches address heterogeneous hallucination drivers: *Object-Aware VCD* preserves attribution-indicated lesion regions while attenuating contextual co-occurrence priors, and *Latent-Disentangled VCD* applies structure-preserving style edits to suppress attribute biases. When neither branch passes the proximity gate, PCCD falls back to greedy decoding, guaranteeing it never degrades below the unmitigated baseline. Across radiology VQA, chest X-ray report generation, and a new CXR existence probe (Med-POPE), PCCD improves GREEN AUC, QAAS, and RadGraph F1 by up to pp over SOTA with one auxiliary forward pass per token and no weight updates.
17.	SpEmoC**: A** balanced speaker-segment multimodal emotion benchmark **S Bano**, S Ahmad, **SK Vipparthi,** S Chanda… - Computer Vision - ECCV 2026, 2026

	Abstract: Understanding human emotions in spoken conversations is a key challenge in affective computing, with applications in empathetic AI, human computer interaction, and mental health monitoring. However, existing datasets vary in scale, emotion distribution, modality alignment, and data partitioning strategies, which can influence reliable cross-dataset generalization and minority-emotion modeling. We introduce **SpEmoC** a **Sp**eaking segment **Emo**tion for **C**onversations comprising 306,544 raw clips from 3,100 English language movies and TV series. From these, 30,000 high quality, class balanced clips are curated, featuring synchronized visual, audio, and textual modalities annotated for seven emotions through a hybrid pipeline that integrates pretrained models with human validation. SpEmoC uses strict movie- and series-level splits to prevent content overlap between split sets, allowing more reliable evaluation of model generalization. The dataset also maintains a near-balanced distribution across seven emotions, including minority classes such as *Fear* and *Disgust*, which supports more balanced learning across categories. Extensive experiments, including in-domain benchmarking, cross-dataset transfer, low-data training, class-imbalance analysis, and modality transfer show that balanced data and careful splitting lead to more stable performance across emotions when models are evaluated on other datasets. These results highlight the importance of dataset design for robust and transferable multimodal emotion recognition.
18.	State-of-charge and temperature-dependent battery parameter identification via 3D polynomial fitting **P Kannojia, A Ahmad, AVR Teja** - 2026 IEEE 6th International Conference on Sustainable Energy and Future Electric Transportation (SEFET), 2026 **Abstract:** This paper presents a technique for Equivalent Circuit Model (ECM) parameter identification of Li-ion batteries through three-dimensional (3-D) plotting and polynomial fitting under varying operating temperature and state-of-charge (SoC). The proposed parameter identification technique, which uses limited data points and requires less memory, can be directly implemented in Battery Management Systems (BMS) at low computational cost. The parameter data of the first-order RC model were analysed using MATLAB, where 3-D polynomial surface fitting was performed with temperature and SoC as input variables and these polynomial fitting equations are directly used to parameter calculation across different operating conditions of SoC and temperature. A goodness-of-fit above 97% is obtained for all the parameters that confirm the accuracy of the proposed fitting method. Owing to its simplicity and efficiency, this approach is well-suited for real-time integration into BMS applications such as state-of-charge (SoC) and state-of-health (SoH) estimation.
19.	Three-phase digital frequency-locked loop based on zero-crossing detection for distorted grid conditions **AVR Teja** - 2026 IEEE 6th International Conference on Sustainable Energy and Future Electric Transportation (SEFET), 2026 **Abstract:** This paper presents a low-complexity three-phase Digital Frequency-Locked Loop (DFLL) based on zero-crossing detection for robust synchronization of grid-connected converters under severely distorted conditions. Unlike conventional PLL-based approaches that rely on coordinate transformations and intensive filtering, the proposed architecture primarily employs a counter-based digital timing strategy driven by a 3.125MHz reference clock, significantly reducing computational burden. The method exploits six zero-crossing events per fundamental cycle to enhance timing resolution and robustness against voltage unbalance and harmonic distortion. The algorithm is implemented in discrete time and evaluated under six disturbance scenarios, including voltage sag, frequency drift, phase jump, dc offset, harmonic injection, and heavy combined

	distortions with high THD levels. Computational analysis demonstrates a significant reduction in arithmetic operations, while achieving frequency settling within 2–3 grid cycles and maintaining frequency ripple within ±1–2 Hz under distorted conditions.
C	**Editorial(s)**
20.	Complex network dynamics of cognitive processing in health and disease: Current knowledge and future research. S Cauzzo…**CK Behera**, SP Muthukrishnan - Frontiers in Computational Neuroscience, 2026 **Editorial Note:** Over the past decade, neuroscience has undergone a profound conceptual shift: rather than ascribing cognitive functions to activations in isolated brain regions, the field increasingly recognizes that cognition emerges from the dynamic interplay of rapidly reconfiguring, distributed neural networks whose efficiency depends on flexible transitions, coordinated integration, and appropriate engagement of internally and externally oriented systems (Faskowitz et al., 2020; Novelli and Razi, 2022; Finc et al., 2026). Advances in neuroimaging and electrophysiology—including EEG, fMRI, MEG, PET, and multimodal combinations—have enabled researchers to characterize brain-network organization across complementary spatial and temporal scales, although each modality captures only part of the underlying dynamics (Lake and Higley, 2022). The evidence spans millisecond EEG states, moment-to-moment fMRI co-fluctuations, multimodal disease-network mapping, motor preparation, and neuroimmune/genomic interactions. The strongest convergence is that disease or increased cognitive demand changes network state transitions, not just regional activity. Simultaneously, advanced computational methods such as graph theory and machine learning offer new frameworks for understanding brain connectivity complexity (Mohammadi and Karwowski, 2024; Yang et al., 2025).
21.	Special issue on sustainable bioinspired design and manufacturing **P Sarkar**, S Sharma, B Chakraborty - Smart and Sustainable Manufacturing Systems, 2026 **Editorial Note:** The increasing urgency of global environmental challenges, resource depletion, and climate change has compelled researchers and industries to rethink conventional approaches to product design and manufacturing. Sustainable manufacturing is no longer merely a technological aspiration but a critical necessity for ensuring ecological balance, economic resilience, and social well-being. In this context, bioinspired design and manufacturing have emerged as transformative paradigms that seek inspiration from natural systems, biological processes, and evolutionary mechanisms to develop efficient, adaptive, and sustainable engineering solutions. Nature generally provides extraordinary examples of optimized structures, resilient systems, and energy-efficient processes which have been developed through millions of years of evolution. By learning from these natural principles, researchers are developing innovative approaches capable of reducing environmental impact and simultaneously improving performance and functionality. Sustainable bioinspired design integrates biological intelligence with advanced engineering, manufacturing technologies, artificial intelligence, and digital systems to create environmentally conscious products and processes. This special issue on “Sustainable Bioinspired Design and Manufacturing” aims to provide a multidisciplinary publication for researchers, academicians, practitioners, and industry experts in the field. Originally, this special issue was conceptualized in response to the growing need for innovative manufacturing solutions that can contribute meaningfully toward the United Nations Sustainable Development Goals (UN-SDGs), particularly those related to responsible production and consumption, industry innovation, sustainable infrastructure, and climate action. The papers included in this issue demonstrate the breadth and diversity of bioinspired sustainable engineering research and also its application in manufacturing. The contributions span healthcare manufacturing, biologically inspired design

	methodologies, robotics, sustainable manufacturing systems, and quality engineering approaches. Together, these studies highlight how inspiration from nature can be translated into practical engineering solutions capable of addressing complex societal and industrial challenges. The opening review article by Kaushik et al. explores the transformative role of additive manufacturing in sustainable healthcare. The paper critically examines how three-dimensional (3D) printing technologies enable localized production, material efficiency, customized medical devices, and reduced waste generation, thereby contributing significantly toward sustainable medical manufacturing ecosystems. The study also discusses challenges related to biocompatibility, regulation, scalability, and environmental impacts associated with nonbiodegradable materials. The paper by Srinivasan and Chakrabarti investigates the influential role of process and product knowledge in biologically inspired design ideation and realization. Their work contributes to a deeper understanding of how systematic frameworks and bioinspired design tools support creativity, concept generation, and prototype realization. The study highlights the importance of combining process-based and product-based knowledge for the successful realization of biologically inspired engineering systems. The contribution by Charu and Gupta presents the design and development of a bioinspired serpentine robotic system intended for excavation and inspection applications. Inspired by snake locomotion, the modular robotic platform demonstrates enhanced maneuverability in constrained and challenging environments. The study by Davinder Singh focuses on integrating Six Sigma methodologies within bioinspired manufacturing systems, particularly in the context of Indian small and medium enterprises (SMEs). The paper identifies critical success factors that influence sustainable manufacturing performance and demonstrates how structured quality improvement frameworks can contribute toward operational excellence and sustainability objectives. This work is particularly valuable for industries aiming to improve competitiveness while minimizing environmental impact. Singh et al.'s paper shows that vegetable oil-based nanofluid minimum quantity lubrication significantly enhances grinding performance and surface quality while reducing environmental and health impacts compared to conventional cooling methods. Kumar et al.'s work demonstrates that recycled PLA reinforced with wood dust can improve thermal and mechanical properties for 3D printing applications, supporting sustainable additive manufacturing. Collectively, the articles in this special issue reflect the growing maturity of sustainable bioinspired research and its practical significance across multiple engineering domains. The issue also highlights the interdisciplinary nature of the field, bringing together concepts from manufacturing engineering, design science, robotics, healthcare technologies, quality engineering, sustainability studies, and digital innovation. We sincerely thank all authors for their valuable contributions and the reviewers for their rigorous evaluation and constructive feedback that significantly improved the quality of the papers. We also express our gratitude to the editorial team of *Smart and Sustainable Manufacturing Systems* and ASTM International for their support in bringing this special issue to fruition. We hope that this special issue will inspire future research, foster interdisciplinary collaborations, and encourage the development of sustainable engineering solutions inspired by the remarkable intelligence of natural systems.
D	**Article(s)**
22.	A bias-driven current injection delay cell based ring VCO with phase noise suppression and -181.7 dBc/Hz FoM_T **MK Singh, U Chichhula**, R Nagulapalli, **DM Das, M Sakare** - IEEE Transactions on Circuits and Systems II: Express Briefs, 2026 **Abstract:** This paper presents a bias-driven current injection delay cell (BD-CI-DC) based ring voltage-controlled oscillator (RVCO). In conventional delay cells, the bias transistor is always ON, which contributes to thermal and flicker noise throughout the oscillation cycle, thereby elevating

	phase noise. The proposed BD-CI delay cell introduces an RC network at the bias transistor, coupled to the input, enabling selective alignment of current delivery. This noise-current shaping in the RVCO reduces the root-mean-square (RMS) value of the output impulse sensitivity function (ISF). Thus, reduces phase noise. A systematic design methodology based on normalized timing characteristics and ISF analysis is presented to guide the selection of the RC network for achieving optimal phase noise reduction. The prototype is fabricated in the standard 65nm CMOS technology, operating at 2 GHz with a 1.2V supply. The measurement results show a phase noise of -93.2 dBc/Hz at an offset frequency of 1 MHz, which is 4.6 dB better than that of a conventional RVCO at a power consumption of 0.61mW. The design achieves figure of merits FoM and FoM_T (including tuning range) of -161.3 dBc/Hz and -181.7 dBc/Hz, which is 2.7 dB and 2.8 dB better than conventional RVCO.
23.	A new efficient framework for reduced two-dimensional nonlinear aggregation population balance models **D Wadhwa, S Yadav**… S Heinrich, **J Kumar** - Chemical Engineering Science, 2026 **Abstract:** Two-dimensional (2D) nonlinear population balance models are inherently complex due to their high computational demands and sensitivity to the choice of grid type. To address the challenge of tracking multiple properties and to provide an alternative to full 2D population balance models, we consider a reduced model that efficiently captures moisture content (tracer) and size distributions of granule in aggregation population balance equations (PBEs), under the assumption that the aggregation kernel depends solely on granule volume and time, and is independent of tracer volume. This reduced model is formulated as a tracer population balance equation (TPBE), for which we present a new and efficient discretization method that ensures conservation of tracer mass. The proposed formulation is versatile and applicable to any grid type, making it suitable for both continuous and batch particulate systems. We validate its performance using two benchmark applications: (a) batch systems and (b) mixed-suspension mixed-product removal systems. The formulation is tested across various kernels and compared against the cell average technique (CAT) to confirm its effectiveness. Results show that the proposed method achieves accuracy comparable to CAT while requiring approximately 50–60% less computational time. Overall, this approach offers a computationally efficient alternative to standard 2D models, with broad applicability in systems where reduced computational cost is critical for particle process modeling.
24.	A novel transient block induced explainable attention W-Net for multimodal medical image segmentation D Pal, **T Meena…**S Roy - Computer Methods and Programs in Biomedicine Update, 2026 **Abstract:** Deep learning has advanced medical diagnostics by enabling automated disease detection and anomaly localization. However, many models remain “black boxes,” as they cannot clearly identify which features drive predictions, limiting clinical trust. This study proposes a framework that ensures both accuracy and interpretability for lesion segmentation and localization in multi-modal medical images. We introduce the eXplainable Attention W-Network (XAW-Net). Its core innovation is a *transient block* connecting encoder and decoder paths through dropout layers following dense convolutional blocks. This design reduces false positives and enhances segmentation precision, particularly for small lesions. For interpretability, we propose Loss-based Gradient Class Activation Maps, which generate layer-wise gradient heatmaps. These visualizations highlight the contribution of individual layers to the final output mask, enabling detailed tracking of network behavior during inference. XAW-Net was evaluated on benchmark datasets across multiple modalities. It achieved Dice Similarity Coefficient scores of 82.3% and 80.7% for breast cancer segmentation in Dynamic Contrast Enhanced and T1 images, 90.2% for

	brain tumor segmentation on the BraTS2020 dataset, 93.8% for breast tumor segmentation from PET images, and 70.8% for cervical fracture localization in the RSNA 2022 challenge dataset. Results demonstrate consistent gains in precision and reduced false positives over conventional architectures. Gradient-based visualizations further confirmed that the transient block improved attention to salient regions while maintaining strong generalization across modalities. In summary, XAW-Net effectively combines accuracy and interpretability for multi-modal medical imaging. Despite variations due to dataset quality and computational demands, it shows strong promise as a reliable and explainable diagnostic aid.
25.	Accelerated GMPP convergence in solar farms via thermal modeling and simultaneous granular string current comparison based evaluation **N Kumar, KR Sekhar** - IEEE Transactions on Industrial Electronics, 2026 **Abstract:** Partial shading reduces energy harvest in photovoltaic (PV) systems by creating multiple peaks on the power-voltage (P-V) curve. Conventional maximum power point tracking (MPPT) methods perform a full curve scan to find the global maximum power point (GMPP), resulting in slow convergence and high computational cost. This work proposes a novel algorithm that exploits the predictable patterns of peak formation under varying irradiance and temperature. The mathematical model uses a strategic three-test-point mechanism, with consideration for temperature extremes, to define voltage variation boundaries. At a defined boundary, the simultaneous string current comparison technique is also introduced to significantly reduce scan points under non-severe shading. By combining temperature-dependent boundary identification with current comparison, the algorithm efficiently narrows the search to a critical fraction of the open-circuit voltage
26.	Accounting for neighbouring effects in measuring the spatial concentration of Indian industries: Evidence from micro-level data S Agarwal, **SR Behera** - Indian Economic Review, 2026 **Abstract:** This paper investigates the role of neighbourhood effects in shaping the spatial concentration of manufacturing and service establishments across Indian districts, using unit-level data from the 2013–14 Economic Census. We apply the spatially weighted Ellison–Glaeser index (EGSPAT) developed by Guimarães et al. (2011) to account for inter-district spillovers in measuring industrial agglomeration. At the national level, incorporating spatial dependence does not significantly alter concentration patterns: highly agglomerated industries remain confined to a small number of districts, with limited spillovers to neighbouring areas. In contrast, state-level analysis for India's three largest employment states—Maharashtra, Uttar Pradesh, and West Bengal—reveals substantial neighbourhood effects. The EGSPAT estimates exceed the standard Ellison–Glaeser index by 8–23 per cent, and districts with excess employment exhibit clear spatial contiguity. These findings highlight the importance of geographic scale in identifying agglomeration dynamics, as national-level measures mask significant within-state spatial dependence. The paper contributes novel evidence for India that spatial spillovers in industrial concentration are primarily a subnational phenomenon, and it underscores the policy relevance of state-level industrial strategies in leveraging localised agglomeration economies.
27.	Analyzing hydrological degradation vulnerability of non-perennial rivers shaped by groundwater stress, geogenic hazard and limited storage potential **T Prashanth, S Ganguly** - Journal of Hydrology, 2026 **Abstract:** Hydrological degradation, which poses a significant threat to river segments in a basin/watershed, manifests as a substantial decline in total water storage (*TWS*) in the river basin owing to rising climatic & anthropogenic stress, and formation of subsurface erosional landforms.

	Assessing and analyzing spatiotemporal variations of hydrological degradation vulnerability (*HDV*) across heterogeneous watersheds remains challenging in data-sparse semi-arid environments. In this context, the present research aims to assess the *HDV* in ungauged river segments using the proposed novel approach (*S4H*). The *HDV* computed using the *S4H* approach is validated using the proposed depth-duration curve-based river aquifer stress index (*DDC–RASI*). The *HDV* estimated by the proposed method is cross-validated using a newly proposed hypsometric-integral-based standardized *TWS* anomaly (*HI–STWSA*) duration curves derived from the Gravity Recovery and Climate Experiment (GRACE) and GRACE Follow-On (FO) satellite missions. To improve spatial patterns of hydrological stress & recovery, the *HI–STWSA* computed at the basin scale is downscaled to the watershed scale. The study finds that certain segments of the Pennar River in southern India exhibit high vulnerability, primarily due to intensive groundwater extraction and extensive sinkhole development, which severely disrupt subsurface storage and flow accumulation. In contrast, the downstream reach of the river near Nellore shows comparatively lower vulnerability, reflecting a lower stage of extraction and better groundwater-surface water connectivity. These findings highlight the urgent need for region-specific water management strategies to mitigate hydrological degradation.
28.	Analysis and design of an optimum CMRR neural amplifier and a figure of merit for noise and area optimization **S Sharma, Shivdeep**, VG Hande, **DM Das** - Integration, 2026 **Abstract:** The neural amplifier presents one of the key bottlenecks in minimizing the power and area of neural interfaces. The neural amplifier's power consumption is mainly constrained by the noise requirement, and its area by CMRR and noise. We propose a novel optimum CMRR neural amplifier (OC-NA) based on a capacitively coupled instrumentation amplifier (CCIA) that enhances CMRR and reduces gain mismatch by a factor of $\sqrt{A_{dm}/2}$for only 50% increase in capacitor area compared to standard CCIA where $A_{dm}$is amplifier gain. An analytical model describing the dependence of the CMRR of a CCIA on the ratio of the OTA's common-mode input capacitance to the feedback capacitor is derived, enabling the selection of the minimum feedback capacitor value without degrading the CMRR. The minimum-value feedback capacitor, area-minimization methodology, and low-mismatch feedback network together minimize area and optimize CMRR and gain mismatch of the proposed amplifier. The post-layout simulation of the OC-NA designed in 180 nm CMOS technology achieves a CMRR of 97 dB mean and 82 dB worst-case without chopping. The OC-NA occupies 0.032 mm^2area, consumes 3.6 µWof power, has 0.045% gain mismatch, and 8.36 µVinput referred noise (IRN) with 4.57 NEF. We also propose a reference amplifier-based figure of merit, Noise and area efficiency factor (NAEF), which captures the trade-off between noise and area of the amplifier. The NAEF of an amplifier can be interpreted as the area it occupies for a given IRN relative to the reference amplifier.
29.	Antioxidant and bone regeneration properties of a hydrogel loaded with gallic acid-functionalized MgO nanoparticles to treat rheumatoid arthritis **Y Thakur, M Kalia, D Pal, Y Singh** - ACS Biomaterials Science & Engineering, 2026 **Abstract:** Rheumatoid arthritis (RA), an autoimmune disorder, is characterized by prolonged joint inflammation that eventually damages it. The overexpression of matrix metalloproteinases along with an influx of inflammatory cytokines in the joint, hyperplasticity of fibroblast-like synoviocytes, and increased levels of reactive oxygen species (ROS) results in an acidic microenvironment that irreversibly destroys the cartilage and bone. Methotrexate is used to treat RA, but it is associated with side effects, like nephrotoxicity and immunosuppression, and there is a lack of drug-free strategies to target the progression of disease and tissue regeneration. To treat RA and promote the regeneration of bone tissue, we have developed a drug-free, oxidized

	chondroitin sulfate-dextran hydrogel loaded with gallic acid-functionalized MgO nanoparticles, which demonstrated promising ROS scavenging and anti-inflammatory activities, as assessed using NO scavenging and reverse-transcription polymerase chain reaction analysis. In addition, the hydrogels were found to promote bone tissue regeneration in cell culture, as determined using the alkaline phosphatase assay and Alizarin red staining along with exhibiting apoptotic potential against hyperplastic fibroblast-like synoviocytes. We report, for the first time, gallic acid-grafted MgO nanoparticles that harness intrinsic antioxidant and apoptotic activity for RA therapy. In summary, we have developed a drug-free, multipotent system for alleviating RA by suppressing inflammation and promoting tissue preservation. 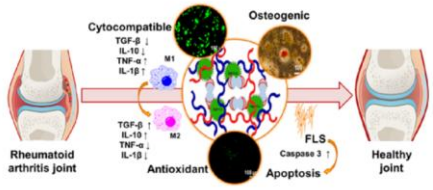
30.	Assessment of collapse behavior and post-collapse compressibility response of soft clay under repeated drying–wetting cycles **G Prasad, M Raheena** - Geotechnical and Geological Engineering, 2026 **Abstract:** Soil collapse is primarily associated with the breakdown of a metastable soil structure, where wetting reduces interparticle bonding and triggers structural rearrangement. While extensive research exists on collapsible silts and loess, the collapse behavior of soft clays subjected to repeated drying and wetting remains under-researched. The present study investigates the effects of six cycles of controlled drying and wetting on the collapse potential, post-collapse compression behavior, and microstructural evolution of a soft organic clay from Kuttanad, a flood-prone coastal region in Kerala, India. Remoulded specimens were subjected to dry–wet cycles of 1-day and 3-day durations and subsequently tested in oedometers, where the soil specimens were allowed to collapse under effective vertical stresses of 50 kPa and 200 kPa. Results show that collapse susceptibility, ranging from moderate to severe, can be caused by repeated drying cycles, with the effect more pronounced under 200 kPa vertical stress and in specimens that underwent 1-day cycles that retained higher water contents. Collapse indices remained significant even at 50 kPa, but were consistently higher at 200 kPa, while the post-collapse compression indices with further loading were higher after collapse at 200 kPa, indicating stress-dependent destabilisation of the partially saturated soil structure. SEM images revealed progressive aggregation of clay domains in the initial cycles and increased inter-aggregate pores with advancing cycles. MIP results indicated that mesopores and micropores were most sensitive to dry–wet cycles and collapse stresses, while ultra-micro and crypto-pores remained relatively stable. Overall, the study highlights that drying–wetting cycles can induce collapsible behavior in soft clays traditionally considered non-collapsible, with implications for infrastructure in regions experiencing intensified seasonal drying and flooding due to climatic variations.
31.	Biaxial strain induced reversible hydrogen storage in 2D boron phosphide biphenylene material **D Dange, P Beniwal, TJ Dhilip Kumar** - ACS Applied Energy Materials, 2026 **Abstract:** The storage of hydrogen energy is the primary obstacle to its widespread use, underscoring the need for efficient storage materials. Motivated by the increasing prevalence of inorganic biphenylene substitutes, strain-induced modulation of hydrogen storage in 2D boron phosphide biphenylene (BPB) via first-principles calculations is investigated. Pristine BPB is an inefficient substrate for hydrogen storage since the adsorption energy is –0.17 eV/H_2, which falls below the DOE requirement. Thus to further enhance the hydrogen adsorption performance, the effect of the strain on BPB monolayer is studied. Compressive strain enhances bond electronic

	density, strengthening H_2 adsorption and increasing adsorption energy. On the application of 1.25% biaxial strain, BPB is able to adsorb 24 H_2 molecules, corresponding to 8.8 wt % storage with an adsorption energy of –0.25 eV/H_2. The occupation number analysis provides an understanding of the hydrogen uptake behavior within the strained BPB complex across different temperatures and pressures. The work emphasizes strained BPB as a versatile reversible hydrogen storage 2D material. 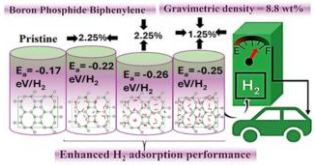
32.	Bifurcation-induced tipping and multistability in a minimal gene regulatory network **SN Chattopadhyay, AK Gupta** - Physica A: Statistical Mechanics and its Applications, 2026 **Abstract:** Cell-fate determination is an inherently multistable process in which cells commit to distinct phenotypic identities, with transitions between these states playing a central role in development and disease progression. Therefore, capturing the nonlinear dynamics that govern such transitions with minimal yet biologically meaningful biophysical models remains a fundamental challenge in theoretical biology. This study aims to examine the nuances of a simplified gene regulatory network comprising two antagonistic transcription factors that self-activate and mutually inhibit each other. Systematic global sensitivity analyses reveal that external activation strength and degradation rates are among the key regulators of the system's steady-state dynamics. Bifurcation analysis further reveals the emergence of tristability, characterised by distinct phenotypic outcomes: two extremes and a hybrid intermediate. Next, the connection between phenotypic switching and the theory of critical transitions is established. After that, a suite of 12 statistical indicators, including classical univariate indicators and various multivariate extensions, is employed to anticipate impending transitions between these phenotypes. The predictive efficacy of these indicators is evaluated across four complementary perspectives: sensitivity, significance, robustness, and false-positive detection. Dimensionality reduction techniques produce indicators that are more sensitive to hyperparameter choices than averaging. Furthermore, statistical significance indicates that most indicators predict critical transitions across cases. Next, the ensemble-level analysis reveals that directly anticipating critical transitions between the two extreme phenotypes is more challenging, whereas the anticipation success improves considerably when the transition proceeds through the hybrid phenotype. Collectively, this work establishes a mechanistic and quantitative framework that links gene regulatory dynamics to critical transition theory, providing insights into the predictability of cell fate decisions.
33.	Carbonaceous catalysts for the hydrolysis of cellulose E Iraianbu, **M Spurthy**, S Chatterjee, B Roy - Carbon Letters, 2026 **Abstract:** Hydrolysis of cellulose, the most abundant biopolymer available, using heterogeneous catalysts remains challenging due to its recalcitrant crystalline structure. Carbonaceous solid acid catalysts, made from low-cost agricultural waste precursors, are emerging as a new alternative to the conventional catalysts, due to their tunable surface chemistry, well-defined porous structures, higher thermal stability under hydrothermal conditions, etc. This paper comprehensively discusses applications of the various carbon materials (biochar, hydrochar, activated carbons, graphene oxide, CNTs, etc.) both biomass derived and commercially obtained, in cellulose hydrolysis. The mass transfer limitations associated with carbonaceous catalysts, the interactions of diverse carbon morphologies with cellulose, the reaction kinetics, AI and ML applications in cellulose hydrolysis using carbon catalysts and the associated research challenges are examined thoroughly. Role of

	various carbonaceous morphologies are compared, and suggestions for future carbon-based catalyst design are presented. Current challenges, including the leaching of the functional groups, raw biomass hydrolysis, and the absence of continuous flow processes, are critically discussed. Additionally future research priorities are identified to guide the field towards commercial biorefinery development.
34.	Catalyst controlled regiodivergent assembly of aminobenzofluorenones **M Kumar, A Kumar, S Devi**, S Basappa…**A Goswami** - Organic Chemistry Frontiers, 2026 **Abstract:** A catalyst dependent (Ag2O versus ZnBr2) protocol has been developed for the regiodivergent synthesis of aminobenzofluorenones either through in-situ generated or isolated ynone tethered with 2-alkynylanilines in good yields. DFT-calculations provide mechanistic insights for the observed regioselectivity. The synthetic utility of products has been demonstrated through derivatization with natural and bioactive acids. The photophysical studies of selected –NMe2 benzofluorenones have also been presented. 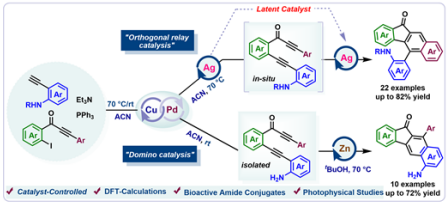
35.	Catalytic transfer hydrogenolysis of lignin models and native lignin over oxygen vacancy–Rich Ni–Ru/HO–TiO_x using isopropanol as a hydrogen donor **A Kumar, R Srivastava** - Energy & Fuels, 2026 **Abstract:** Developing sustainable and hydrogen-efficient catalytic strategies for lignin valorization remains a significant challenge for renewable energy and environmental applications. Herein, we report a defect-engineered, oxygen vacancy–rich Ni–Ru/HO–TiO*x* catalyst for selective catalytic transfer hydrogenolysis (CTH) of β-O-4 lignin model compounds and native hardwood lignin into value-added chemicals and fuels. Surface hydroxyl enrichment and oxygen vacancies are proposed to enhance metal–support interactions, hydrogen spillover, and C–O bond activation over the optimized 3Ni1Ru/HO–TiO*x* catalyst. Using isopropanol as both solvent and hydrogen donor, the catalyst achieved >99% conversion of 2-phenoxy-1-phenylethanol at 160 °C, with tunable selectivity toward aromatic and cyclic hydrocarbons in the absence of externally supplied molecular hydrogen. Mechanistic and kinetic studies suggest that in situ alcohol dehydrogenation, defect-rich interfaces, and modulated surface acidity facilitate hydrogen transfer, selective ether bond cleavage, and controlled hydrogenation. The catalyst showed good stability, recyclability, and minimal metal leaching. Furthermore, the catalytic system upgraded organosolv hardwood lignin into C_6–C_9 cyclic hydrocarbons. CHEM21 green metrics analysis indicated improved material efficiency and reduced environmental impact under optimized conditions. These findings demonstrate the potential of defect-engineered catalysts for sustainable lignin upgrading using catalytic transfer hydrogenolysis pathways. 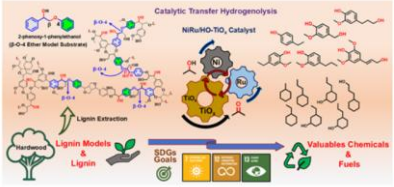
36.	Compact model for uniaxial strain-induced threshold voltage shift in high-k/metal gate nanoscale bulk MOSFETs **Y Swami** - Russian Microelectronics, 2026

	Abstract: This paper presents a physics-based compact model to analyze the impact of uniaxial strain on the threshold voltage (VTH) of nanoscale bulk strained-silicon (SS) MOSFETs with high-k dielectrics and metal gates. Unlike most existing models that primarily address axial strain, the proposed model uniquely incorporates both axial and normal strain components, thereby capturing the full directional impact of mechanical stress on the channel. This comprehensive approach enables a more accurate prediction of threshold voltage shifts, especially at nanoscale dimensions where normal strain becomes increasingly influential. The model also accounts for critical process parameters, including gate length, gate height, gate width, stress liner thickness, intrinsic stress, and offset spacer geometry. A virtual decomposition of the stress liner regions is employed to capture both direct and indirect stress transfer mechanisms. The final VTH model is expressed using only four fitting parameters, enabling physically insightful and computationally efficient prediction of strain-induced threshold voltage shifts. The model is validated against independent experimental data and calibrated 2D TCAD simulations across various technology nodes. It is broadly applicable to bulk, SOI, PD, and FinFET architectures and can be seamlessly integrated into TCAD environments for compact modeling and circuit design.
37.	Conformationally restrained *de novo* peptides to modulate Skp1–Skp2 interaction of the SCF E3 ligase S Tolani, **NM Tripathi**, H Antil, S Ghosh…**A Bandyopadhyay** - RSC Medicinal Chemistry, 2026 **Abstract**: Skp2, the substrate-recognition component of the SCF ubiquitin ligase complex, has been widely implicated in oncogenesis across diverse malignancies, positioning it as a compelling therapeutic target. The protein–protein interaction interface of Skp1–Skp2 offers an effective intervention point, as disruption of this interaction can impair the ability of Skp2 to identify and bind to its downstream substrates. However, inhibiting this interface with small-molecule inhibitors poses considerable challenge. Here, we introduce de novo peptide sequences through in silico screening of a peptide pool to target the Skp1–Skp2 core interface. The screening identified four linear precursors, which were further conformationally restricted to increase affinity and conformational stability by deploying cysteine-mediated late-stage crosslinking. Biophysical and cellular analyses of these crosslinked peptides revealed candidate peptides, P2SS and P4SS, which bind effectively to the desired interface and reduce Skp2 protein expression. Skp2 reduction further attenuates p27 ubiquitination, leading to the accumulation of p27 and subsequent G0/G1 cell-cycle arrest, ultimately resulting in cell death. Collectively, our findings establish the potential of first-in-class peptides in targeting the Skp1–Skp2 interface for the treatment of cancers driven by Skp2. 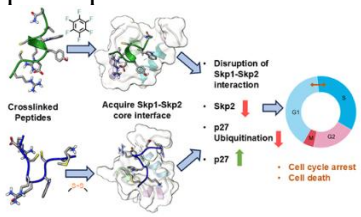
38.	Critical internal pressure for passive failure of shallow pressurized rock caverns/tunnels **R Ganesh** - Géotechnique Letters, 2026 **Abstract:** The assessment of passive failure of a pressurized storage cavern or tunnel in a rock mass is important for determining the required rock cover thickness (or overburden depth). This study proposes a semi-analytical solution procedure based on the kinematic approach of limit analysis to determine the critical internal storage pressure required to induce passive failure of a long flat-ceiling pressurized cavern or tunnel overlain by a shallow rock mass layer. The analysis

	is based on a single-wedge failure mechanism with a curved rupture surface, and the rock mass strength is characterized using the generalized Hoek–Brown (GHB) failure criterion. The shape of the rupture surface is governed by the scaled Mohr envelope of the GHB failure criterion expressed in parametric form. Using the work–energy balance expression, the least kinematic solution is obtained through a minimization procedure with respect to a single parameter that defines the complete geometry of the failure mechanism. The results are expressed in terms of the dimensionless critical storage pressure for various dimensionless parameters governing rock mass behavior, the rock cover thickness ratio, and the surcharge pressure ratio. The proposed method yields solutions that are in close agreement with existing studies.
39.	Cu-doped Ga_2O_3 thin films enabling high-performance p-type solar-blind photodetectors **M Pradhan, Shivani, A Sharma**, CB Auti…**V Shukla**… - ACS Applied Electronic Materials, 2026 **Abstract:** Low hole mobility, strong hole trapping, and self-compensation effects limit the achievement of stable p-type conductivity in the β-Ga_2O_3 semiconductor, thereby inhibiting its application in advanced electronic devices. From a theoretical standpoint, the relatively flat nature of the valence band maximum (VBM) with dominant oxygen vacancy-related donor states constitutes a major bottleneck that intrinsically drives the material toward n-type conductivity. In this study, we successfully achieved p-type conductivity in gallium oxide thin films using copper doping. The introduction of controlled Cu as an acceptor dopant using RF magnetron sputtering into the Ga_2O_3 film facilitates bipolar transport by creating an acceptor impurity level near the valence band maximum (VBM), resulting in conductivity modulation. X-ray photoelectron spectroscopy (XPS) and capacitance–voltage (*C–V*) measurements provide evidence of p-type conduction with a high hole concentration on the order of $10^{19}cm^{-3}$. The positive Seebeck coefficient (*S*) further confirms hole-dominated electrical transport. Moreover, theoretical analysis reveals that the Cu-induced localized states near the VBM predominantly originate from Cu-d states hybridized with O-p states, indicating strong local Cu–O interactions at the octahedral sites and providing microscopic insight into the experimentally observed modulation of electrical conductivity. Finally, a solar-blind photodetector was fabricated using optimized copper-doped p-type gallium oxide thin films. The fabricated device demonstrates remarkably high performance with a photo-to-dark current ratio (PDCR) of 157.33 ± 0.88, responsivity of 806.88 ± 20.55 A/W, external quantum efficiency of (4.01 ± 0.10) × 10^5%, noise-equivalent power of (1.88 ± 0.01) × 10^{-13} W $Hz^{-1/2}$, and a specific detectivity of (2.58 ± 0.05) × 10^{12} Jones at 250 nm with a moderate bias of 5 V at a 1 Hz frequency, demonstrating consistent performance across five nominally identical devices. These findings show that the interfacial electrostatics and charge-transport mechanisms in Ga_2O_3 Schottky devices are efficiently tuned by regulated Cu inclusion, offering insights for enhancing ultra-wide-bandgap oxide-related devices. 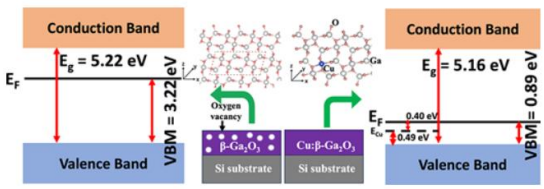
40.	Data-driven design and optimization of electromagnetically crimped multi-material tubular joints A Chetry, **M Agrawal**, A Nandy - Journal of Materials Engineering and Performance, 2026 **Abstract:** Multi-material joining technologies require substantial development to fully harness the benefits of combining several useful constituent material properties in a single component. Electromagnetic crimping (EMC) provides a high-strain-rate, solid-state alternative to

	conventional joining methods. However, predictive modelling and optimization of EMC joints have not been explored much due to the high computational cost of coupled FEM simulations. This work presents an integrated optimization framework combining an automated FEM data-generation scheme, learning-based surrogate models, and particle swarm optimization (PSO). ANN models are trained using axisymmetric FEM for EMC with smooth profiles, while a transfer learning (TL)-based surrogate effectively handles complex threaded profiles. This TL-based surrogate model leverages the advantages of an approximate axisymmetric model and accurate 3D FEM simulations. We have compared the model prediction with the experimental data to ensure the practical utility of the developed model. The proposed data-driven PSO optimization scheme predicts optimum design parameters that improve the joint strength significantly for both smooth and threaded base tube profiles. These highlight the potential of the proposed framework to provide fast, accurate, and scalable design support for EMC-based multi-material joining.
41.	Development of a comprehensive sustainability index for micro-EDM in blind micro hole fabrication using multi-criteria decision analysis S Pratap, **P Kumar**, P Anand, RK Upadhyay - Transactions of the IMF, 2026 **Abstract:** Blind micro-hole fabrication by micro-electrical discharge machining (micro-EDM) is limited by one-directional flushing: debris cannot leave the far side of the workpiece and recirculates through the gap, penalising surface integrity, dimensional accuracy and energy efficiency simultaneously. Existing studies treat these penalties as independent objectives and offer no scalar metric for parameter selection. This paper develops a Composite Sustainability Index (CSI) that fuses nine technical, economic, environmental and social indicators into a dimension-free score bounded by 0 and 1. Weights are derived by the Analytic Hierarchy Process from a seven-member expert panel (consistency ratio 0.019) and runs are ranked by TOPSIS. Validation uses a Taguchi L9 experiment on Ti-6Al-4 V with a 100 µm copper electrode and three dielectrics: distilled water, EDM oil and a 50:50 (v/v) mixture. The best condition (pulse-on time 2 µs, peak current 1.0 A, mixed dielectric) reaches a CSI of 0.637. Technical criteria carry 47.1% of the weight and surface roughness alone explains 38.4% of the inter-run CSI variance, while analysis of variance attributes 43.9% of that variance to dielectric choice. Cross-validation against GRA, VIKOR and MOORA and ±15% weight perturbations (Spearman $\rho > 0.88$) confirm rank stability. The framework is materials-agnostic and needs no extra instrumentation.
42.	Early detection of slow-moving landslides in the Himalayas and Western Ghats using PSInSAR **A Shylu, RK Tiwari, N James,** B Pradhan, **V Sood** - Geomatics, Natural Hazards and Risk, 2026 **Abstract:** Landslides are major natural hazards in mountainous regions, such as the Himalayas and Western Ghats. Rainfall-induced slope failures in these regions exhibit a seasonal recurring nature and pose a serious threat to life and property. Understanding landslide occurrences and their relationship with ground and climatic parameters is therefore important for mitigating their impact. This study investigates slope deformations with persistent scatterer interferometric synthetic aperture radar (PSInSAR) time series analysis using Sentinel-1 images. This study employs a detailed site monitoring strategy for slow-moving slopes or reactivation sites susceptible to slow movement. This study proposes a statistical framework to quantify movement transitions in persistent scatterer (PS) groups. However, limited studies have systematically quantified movement transitions within PS groups to understand pre-failure deformation behaviour in slow-moving landslides. This study addresses this gap by developing a statistical framework to detect early deformation signatures, advancing current PSInSAR applications for landslide early warning. A comparative study of spatiotemporal deformations revealed characteristic movement patterns. Monitoring the PS of the slow-moving zones exhibits desynchronized deformation within slide zones marked by transitions in contrast to the neighbourhood. The study also identified

	transition periods that precede landslides and correlate with rainfall, highlighting the potential for early detection.
43.	Eco-evolutionary decoupling drives silent ecosystem collapse in the Anthropocene **DA Mosoh** - Frontiers in Climate, 2026 **Abstract:** Conservation science has long inferred ecosystem stability from static properties such as species abundance and diversity, assuming ecological and evolutionary processes operate on separable timescales. This foundational assumption no longer holds. Rapid climate change-manifested through sustained warming, altered precipitation regimes, ocean acidification, and the increasing frequency and intensity of extreme events such as heatwaves, droughts, and marine heatwaves—now acts as a dominant global driver simultaneously disrupting ecological function and imposing strong, novel selection on contemporary populations (Faillace et al., 2021; Mosoh, 2026; Mosoh et al., 2024; Reusch and Wood, 2007). Unlike other anthropogenic stressors, climate change operates through both directional trends and acute pulse disturbances, compressing ecological and evolutionary timescales into the same temporal domain while imposing rate-dependent constraints on adaptive responses. Under these conditions, ecological dynamics drive rapid evolution while evolved traits immediately reshape ecological interactions, generating tightly coupled eco-evolutionary feedbacks that govern system trajectories in real time (Govaert et al., 2019). However, when the rate of climate-driven environmental change—particularly under extreme events—exceeds the capacity of interacting species to adapt, ecological and evolutionary processes cease to track one another, initiating eco-evolutionary decoupling. This temporal compression and subsequent decoupling fundamentally alter how ecosystem collapse unfolds. Demographic stability can persist even as adaptive capacity erodes. Populations may decline demographically while retaining high genetic diversity ("drift debt"), or remain numerically abundant while carrying genomic signatures of future maladaptation ("genomic vulnerability") (Bay et al., 2018; Liu et al., 2025). Under climate change, such mismatches are amplified by shifting thermal niches, altered hydrological regimes, and increasing climatic variability, which generate persistent lag loads and maladaptive trait-environment relationships. At the community scale, network feedback can drive systems toward tipping points even when species richness remains high (Huang et al., 2021). Climate-driven restructuring of species interactions—via phenological shifts, altered metabolic constraints, and environmentally mediated changes in species performance—further intensifies this instability. Because interaction outcomes themselves are now evolutionarily labile—shifting along mutualism-antagonism continua and restructuring ecological networks—species interactions, not just species numbers, become the primary locus of destabilization (Mestre et al., 2024; Strona, 2022). Rapid trait evolution can reconfigure pollination systems, host-parasite dynamics, and microbial symbioses over ecological timescales, directly altering the interaction architecture that sustains ecosystem function (Li et al., 2021; Mackin et al., 2021). Here, an integrated framework is advanced in which accelerating co-evolutionary dynamics decouple ecological and evolutionary feedbacks (**Figure 1**). Climate-driven environmental change reshapes selective landscapes simultaneously across interacting species, producing multi-trait, multi-species responses that are frequently non-stabilizing, particularly under rapidly shifting or extreme climatic conditions. Microbiomes may buffer hosts against stress or instead impose physiological constraints when symbionts fail (Hoang et al., 2021; Renoz et al., 2019), while phenotypic plasticity can maintain short-term abundance yet mask declining adaptive potential (Aguirre and Manrubia, 2015). Extreme climate events are especially critical in this context, as they impose abrupt selective filters that can overwhelm plastic and evolutionary buffering, generating rapid transitions from apparent stability to functional breakdown. Historical contingency embedded in latent genetic variation may further lead to abrupt shifts in traits or interactions when environmental thresholds are crossed (Freund, 2023). This produces hidden phases of collapse detectable only through genomic and network-level signals, rather than static

	biodiversity metrics. Such transitional states include genomic–demographic mismatches, plasticity traps, ghost transients arising from delayed system responses, and connectivity fragmentation preceding local decline (Aguirre and Manrubia, 2015; Hand et al., 2015; Sardanyés et al., 2024). Under accelerating climate change, these hidden states may become increasingly prevalent, as systems are forced beyond historical adaptive regimes while maintaining transient structural stability. Detecting them requires dynamic indicators—temporal genomic trajectories, rates of allele-frequency change, and shifting network topology—rather than static snapshots of abundance or diversity. By explicitly linking eco-evolutionary decoupling to the rate, variability, and extremity of climate change, ecosystem collapse is reframed as a climate-driven, rate-dependent process unfolding before observable biodiversity loss. By reframing ecosystem collapse as a dynamic process unfolding before extinction becomes visible, this analysis argues for a predictive science of eco-evolutionary tipping points capable of detecting and managing instability while recovery remains possible. 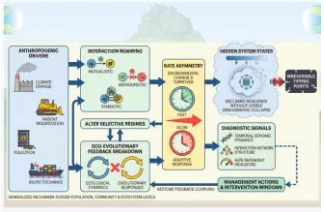
44.	Effect of synthesis parameters on the morphology and mechanical behaviour of vertically aligned carbon nanotube arrays **V Kumar**, A Patel, S Basu, **PK Agnihotri** - Applied Physics A, 2026 **Abstract:** Vertically aligned carbon nanotubes (VACNTs), often called turfs or forests, find applications in thermal interface materials, electro-mechanical probes, and energy absorption devices. Understanding the collective mechanical behaviour of the CNT networks is therefore of significant technological interest. The synthesis parameters and protocols adopted determine the quality of the VACNT forest. We have performed a systematic experimental study to establish the relationship between key synthesis parameters (catalyst thickness, flow time and flow rate of carbon source) and stress bearing capacity of VACNT forests grown using fixed-catalyst chemical vapour deposition technique. We have grown tall VACNT arrays using optimal growth conditions. Results indicate that beyond a critical flow time of the source gas, the height of the obtained VACNT arrays reach a maximum and their stress bearing capacity drops significantly. Simple Finite Element simulations suggest that strong gradient of stiffness develops along the height of the array.
45.	Emerging two-dimensional vdW materials and their heterostructures for memristive devices: advances, challenges, and perspectives **Shiksha, M Kumar** - Advanced Materials Technologies, 2026 **Abstract:** The continuous scaling of conventional CMOS technology has posed critical challenges for modern electronic systems, including high power consumption and limited memory density. The major challenge in current computing systems is the von Neumann bottleneck, which arises from frequent data transfers between memory and computing units, resulting in increased power consumption. These issues emphasize the importance of memristors as next-generation electronic devices capable of meeting the growing demand for energy-efficient and high-performance computation. Memristors provide a solution by combining memory and calculation within a single device, offering nonvolatile data storage and resistance modulation. Researchers explored next-generation 2D vdW materials and their heterostructures as resistive materials for memristors. Here, we present the current advances in memristors based on 2D vdW materials and their heterostructures. Also, analysing their critical resistive-switching behavior under external bias and

	their suitability for various applications. This review highlights key performance metrics, including power consumption, endurance, retention time, On/Off ratio, and their dependence on material properties and device architecture. Finally, conclude with challenges that limit reliability, scalability, and long-term stability, thereby hindering practical implementation. Furthermore, the existing gaps in memristor research are highlighted, and possible strategies and solutions are proposed to enable the device's realization for future prospects.
46.	EngageNet++: Affective integration and interpretable multimodal engagement prediction **M Singh**, X Hoque, D Zeng, Y Wang, K Ikeda, SS Khan, A Dhall - IEEE Transactions on Affective Computing, 2026 **Abstract:** User engagement refers to the level of involvement, enthusiasm, and emotional investment individuals show while interacting with a system. Building engagement prediction systems for real-world settings requires learning from diverse and representative data. Modeling engagement from video is non-trivial, as the cues occur at different time scales. Our previous work introduced the EngageNet dataset for engagement prediction. However, our earlier modeling approaches used single temporal paths, which may not capture both short-term and long-range dependencies. It was also not clear which observable cues mattered most. In this work, we extend that framework and present EngageNet++, a strong, affectively grounded, and interpretable baseline for engagement prediction. It fuses Temporal Convolutional Network (TCN) and Transformer models in parallel to capture both short-term behavioral dynamics and long-range temporal dependencies, and enriches the representation with affective features alongside structural and statistical facial descriptors. We evaluate it on the EngageNet and EngageWild datasets across classification and regression tasks, and provide a systematic analysis of which behavioral and affective cues are most predictive of engagement and under what conditions. EngageNet++ also provides feature-level and attention-based interpretability, highlighting the affective and visual cues most influential to engagement. Additionally, we analyze the effects of users' familiarity with stimuli content, and how engagement varies with user interest across diverse video stimuli. Overall, EngageNet++ bridges predictive performance and interpretability, enabling deeper insights into the cues driving user engagement.
47.	Engineering [7]helicene *via* peripheral boron–nitrogen Lewis pair fusion: from synthesis to cellular imaging **SS Bisht, N Kumar, P Kashyap, H Chhabra, JN Agrewala, AC Shaikh** - Journal of Materials Chemistry B, 2026 **Abstract:** The judicious incorporation of main group elements such as boron–nitrogen Lewis pair motifs into π-conjugated frameworks has emerged as a powerful strategy for developing novel functional hybrid materials with significant potential for application in biological and materials chemistry. Herein, we report the concise synthesis and comprehensive photophysical characterization of a boron–nitrogen fused [7]helicene, which shows emission in the yellow–green region, prolonged fluorescence lifetimes, and redox activity. Single-crystal X-ray diffraction studies confirm the coexistence of P- and M-helical enantiomers, which adopt an ordered heterochiral packing arrangement in the solid state. Furthermore, the helical boron–nitrogen adduct was investigated in cell imaging studies, where it exhibits enhanced intracellular photostability, lower cytotoxicity, and effective staining of cytoplasmic compartments. Additionally, to gain insight into its electronic structure and frontier molecular orbital energetics, density functional theory (DFT) calculations were performed.

	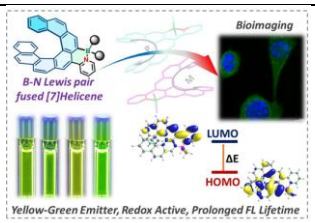
48.	Exchange rate and pass-through under alternative monetary policies: Evidence from India **SA Shah, B Garg** - Review of International Economics, 2026 **Abstract:** This article examines the role of alternative monetary policy rules in shaping exchange rate pass-through and macroeconomic dynamics in a small open economy. To this end, we develop and estimate a Bayesian dynamic stochastic general equilibrium model featuring a conventional monetary policy rule and an exchange rate-augmented monetary policy rule. The results show that incorporating exchange rate movements into the monetary policy rule lowers exchange rate pass-through and weakens the transmission of external shocks to domestic inflation. Results from impulse response and conditional variance decomposition analyses reveal that the exchange rate-augmented monetary policy rule enhances the economy's resilience to external disturbances. In addition, recursive forecasting shows comparable predictive performance under both policy rules, albeit modest improvements in interest rate forecasts under the exchange rate-augmented monetary policy rule. Counterfactual analysis further complements the empirical relevance of the exchange rate-augmented monetary policy rule. Policy-wise incorporating exchange rate considerations into monetary policy can strengthen macroeconomic stability and policy transmission in small open economies such as India.
49.	Experimental investigation and statistical modelling of cutting temperature with surface and tool morphological analyses in laser-assisted turning of Inconel X-750 S Shaik, G Punugupati, **R Kant**…CSP Rao - Proceedings of the Institution of Mechanical Engineers, Part E: Journal of Process Mechanical Engineering, 2026 **Abstract:** Inconel X-750 is extensively used in aerospace, nuclear and power generation industries because of its excellent mechanical strength and oxidation resistance at elevated temperatures. However, its high strength, work-hardening tendency and poor thermal conductivity make conventional machining difficult. Laser-assisted turning (LAT) has been widely adopted to improve the machinability of hard-to-cut materials. The influence of machining parameters on cutting temperature and the associated changes in surface and tool morphology during LAT of Inconel X-750 have not been systematically investigated. In this study, LAT experiments were performed on Inconel X-750 using a Taguchi L27 orthogonal array by considering laser power, spindle speed, feed rate and depth of cut (DoC) as the machining variables, with cutting temperature selected as the primary response. The experimental data were analysed using analysis of variance and regression analysis to establish the relationship between machining parameters and cutting temperature. Scanning electron microscopy and microhardness measurements were used to characterize the machined surface and cutting tool. Laser power had the greatest influence on cutting temperature, contributing 84.11%, followed by DoC (6.38%). The regression model showed good agreement with the experimental results, with an R^2 value of 97.57%. The validation test confirmed the model with an accuracy of 94.83%. Moderate cutting temperatures produced more uniform surface morphology, whereas excessive temperatures promoted material smearing, adhesion and diffusion-related changes on the cutting tool. LAT reduced the microhardness because of thermal softening, although the hardness remained above the annealed condition of the alloy.

50.	FMFT: A memory-augmented multi-feature fusion transformer enhanced with retrieval augmented graph-based few-shot learning **S Chauhan**, S Saxena, **S Jain**, D Parashar - IEEE Access, 2026 **Abstract:** Indic text is syntactically compact, semantically ambiguous, and highly context-dependent, making English translation particularly challenging. Traditional neural machine translation (NMT) methods, even when enhanced with pre-trained language models (PLMs) and linguistic features such as part-of-speech (POS) tags, syntactic dependencies, and semantic role labels (SRLs), struggle to generalise in few-shot settings and often lack consistency across language structures. To address the above limitations, this work proposes a Few-Shot Memory Fusion Transformer (FMFT). The FMFT is a memory-augmented, multi-feature-fusion transformer enhanced with the Retrieval-Augmented Graph (RAG) and Few-Shot learning. FMFT combines multi-granular linguistic signals with a graph-structured semantic memory network, in which nodes represent key tokens (e.g., phrases, named entities) and edges represent purely syntactic, semantic, and contextual relationships. A graph-based dynamic retrieval mechanism that uses Personalised PageRank and a minimum-cost spanning tree enables on-the-fly retrieval of context for each translation instance. This is fused with PLM features via a gated, attention-based multi-feature fusion module that adaptively balances linguistic signals. A multi-head memory attention mechanism incorporates this information into the decoder to enhance semantic clarity and long-range dependency handling. FMFT also learns through non-parametric continual learning with a scalable long-context memory buffer. It adapts to various evolving language inputs without requiring retraining. Evaluation of five Indic-English corpora reveals that FMFT significantly outperforms competitive baselines in both full-resource and few-shot scenarios, achieving improvements in BLEU, ROUGE, METEOR, and Chrf scores. Its handling of rare or ambiguous constructs makes it particularly effective for translating low-resource historical languages. At the same time, its modular graph-based design supports scalability, interpretability, and reuse for domain-specific translation tasks.
51.	Fractal dimension of the void field as a compact descriptor of ductile void damage in FCC metals **S Dixit, A Tiwari** - Materials Letters, 2026 **Abstract:** Ductile damage is usually quantified through the void volume fraction (VVF), but measuring it on a section is limited by imaging resolution and says nothing about how the voids are arranged. We section tensile specimens of OFHC copper, ETP copper and SS316L along the gauge and measure VVF against local true strain, showing that the box-counting fractal dimension D of the void field tracks it within every specimen (r = 0.92 to 0.99). The damage rate d(VVF)/dε ranks the materials 0.70 (ETP copper) > 0.52 (OFHC copper) > 0.16 (SS316L), set by oxide-particle nucleation in ETP copper and by matrix strength in SS316L. D is a compact empirical descriptor obtained from the mask that already yields VVF; we state the box-size interval over which it is fitted and claim neither a demonstrated scaling regime nor transferability between magnifications. A gliding-box lacunarity from the same mask falls as the void fraction rises (r = −0.52). 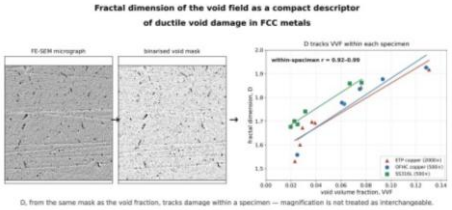

52.	From clustering to global synchrony: Higher-order interactions reshape ecological network dynamics **A Narang, PS Dutta** - Physical Review E, 2026 **Abstract:** The complexity of many natural systems stems from the abundance of interactions that go beyond simple pairwise networks. While higher-order interactions (HOIs) are fundamental to the dynamics of complex networks, their role in shaping ecological communities through species dispersal remains poorly understood. Here, using chaotic tritrophic dynamics, we explore how synchronization emerges in networks characterized by both dyadic and three-body interactions. In random networks, HOIs reduce extreme asynchrony by promoting partial clustering, but never produce complete synchrony. By contrast, in globally connected networks, stronger HOIs drive the system from asynchronous states to full synchrony, with important consequences for community persistence. Employing the master stability function, we further demonstrate that global synchrony remains stable once a critical coupling threshold is crossed. Our findings reveal that HOI-mediated dispersal introduces topology dependence governed by the local triadic structure of the landscape network, which critically shapes the system's collective emergent dynamics. 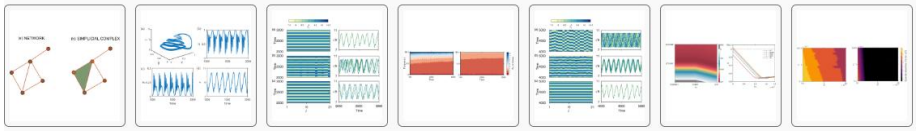
53.	Gelatin methacrylate as a mesenchymal stem cell delivery vehicle: Experimental and semi-quantitative evaluation under metabolic stress **P Yadav, A Mukherjee, B Das** - Macromolecular Bioscience, 2026 **Abstract:** Stem cell-based therapies derived from various sources hold significant potential in regenerative medicine due to their unique properties, particularly their ability to differentiate, self-renew, and modulate the immune system. A polymer-encapsulated Mesenchymal stem cell (MSC) approach can create protective environments for stem cells, enhancing overall therapeutic efficacy. Gelatin Methacrylate (GelMA) is used as a model extracellular matrix to encapsulate MSCs for potential applications in cell-based therapy and bioprinting. This study aims to understand the limitations of GelMA-encapsulation-based cell therapy for an injured tissue. Due to the harsh microenvironment at the implantation site, directly injected stem cells for treatment are affected by factors such as nutrient and oxygen deprivation, immune rejection, reduced cell retention, and inflammatory cytokines. In the current study, we tried to mimic this system. We optimized the GelMA hydrogel cell-encapsulation composition from synthesis through physicochemical characterization, and then tested its cytocompatibility with MSCs. We have further performed numerical modeling to understand and control the behavior of MSCs within the 3D GelMA hydrogel construct under varying metabolic and immunological stress microenvironmental conditions, thereby optimizing the boundary conditions of GelMA-based cell delivery systems.
54.	Geospatial data integration and field assessment techniques for optimizing landfill site suitability in high-altitude tourist areas in the Indian Himalaya R Gellu, **S Sharma…RK Tiwari** - Physics and Chemistry of the Earth, Parts A/B/C, 2026 **Abstract:** The rapid urbanization and population growth in Himalayan towns is often coupled with the absence of authorized landfill site, leading to widespread open dumping, which poses severe environmental and public health risks. The process of landfill site selection is inherently complex due to the interplay of multifaceted and often conflicting administrative, social, technical, environmental, and economic factors. An integrated and advanced geospatial analysis using

	decision-support framework, and Multi-Criteria Decision-Making (MCDM) methodologies can systematically assess and optimize landfill site selection within ecologically fragile and topographically challenging terrains. In the present study, a famous tourist destination i.e. Manali town of Himachal Pradesh, India is the focal point for advanced landfill siting by integrating environmental suitability with economic and regulatory factors to identify implementation-ready waste management sites. Field investigations were conducted to map; waste collection points, evaluate segregation practices, and assessing the landfill operational efficiency in the study area. A land suitability analysis was performed by incorporating key environmental and socioeconomic parameters including, topography, hydrogeology, land use/land cover (LULC), ecological sensitivity, and settlement proximity. The study introduces a scientifically rigorous and policy-relevant approach by employing the Land Suitability Index (LSI) to evaluate environmental feasibility and the Total Waste Towing Distance (TWTD) analysis to assess economic viability of selected landfill sites. The analysis identified 8 potential landfill sites in the study area with highest suitability index values of 0.206 and 0.197 for sites A in Village Bran and site D in Village Badgram respectively. The average waste towing distance analysis from total 253 collection sites to the potential landfill sites in the study area highlighted site G in village Shaleem and site E in Village Pujan as the most economically viable landfill sites. The findings provide an evidence-based, resilient, and adaptive framework for sustainable landfill site selection, minimizing ecological and tourism-related impacts while enhancing overall waste management efficiency. This research contributes to the analysis of sustainable waste management and its intersection with the relevant sustainable development goals (SDGs) for an emerging populated Higher Himalayan town.
55.	Geospatial mapping, risk assessment and multivariate analysis of naturally occurring radionuclides and potentially toxic elements in agrarian soils of SAS Nagar, Punjab, India **SS Kaintura**… **N Kaur, S Kaur**, FM Van der Zwan, **PP Singh** - Scientific Reports, 2026 **Abstract:** Rapid urbanization, industrialization, and agricultural advancements underscore the need to monitor environmental radionuclides and potentially toxic elements (PTEs) for pollution and human health impact assessment. This study assessed human health risks associated with radionuclides and PTEs in agricultural soils of the SAS Nagar District, Punjab, India, using ICP-MS and XRF techniques. Mean radionuclide concentrations were found to be 34.7 ± 3.1 Bq kg^{-1} (^{238}U), 56.5 ± 8.4 Bq kg^{-1} (^{232}Th), and 556.8 ± 93.1 Bq kg^{-1} (^{40}K), respectively, with levels all above corresponding global means. Elemental concentrations (ppm) followed a decreasing sequence: Fe (29,148) > > Zn (67.4) > Cr (55.7) > Ni (25.5) > Cu (23.4) > Pb (18.6) > Th (13.9) > Co (8.8) > As (6.5) > U (2.8) > Cd (0.17). Pollution indices identified As and Cd as the dominant contributors to soil contamination, with U and Cr exerting moderate secondary effects. A multi-pathway exposure model indicates carcinogenic risks within the permissible range; however, As, Cr, and Ni remain within tolerable limits (10^{-6}–10^{-4}) but still signify potential concern. IDW-based spatial mapping of selected radionuclides and PTEs revealed zones of co-contamination across the study area. Spearman's rank correlations show strong to very strong monotonic relationships among most soil variables. Principal Component Analysis (PCA) showcased that the first three components explained a major portion (78.2%) of the total variance. PCA separates variables driven by common environmental processes from those influenced by geogenic and anthropogenic factors, while Hierarchical Cluster Analysis (HCA) groups parameters with similar behavior reflecting these controls. Collectively, these findings emphasize the need for targeted soil quality monitoring to safeguard long-term soil quality and public health.
56.	Greybody factor in AdS black brane spectroscopy: a study with scalar and electromagnetic perturbations A Bhatta, **A Maurya** - Journal of High Energy Physics, 2026

	Abstract: We compute the greybody factor for scalar and photon radiations in AdS Schwarzschild black brane. We consider the linearized field equations satisfied by the minimally coupled massive scalar field and the transverse components of the Maxwell fields on the black brane background and recast them to the Heun's equations by appropriate change of variables and field redefinitions. At the asymptotic region, we consider appropriate linear combinations of the normalizable and non-normalizable solutions of the field equations to construct in/outgoing modes. We consider the ingoing solutions near horizon to construct the IN state and compute the coefficients of the in- and outgoing modes of the asymptotic solutions in terms of the connection coefficients of the Heun functions. Finally by calculating ratio of the coefficient of outgoing modes to the ingoing modes we find an exact expression for the greybody factor. We find that the greybody factor for the transverse Maxwell fields and that for the scalars dual to the conformal scalar primaries with integer scaling dimensions vanish off.
57.	High-temperature oxidation of CoCrFeMnNi-and AlCoCrFeNi-based high-entropy alloys: A critical review on mechanisms, kinetics, and alloy design principles **D Singh, H Singh, R Kumar** - High Temperature Corrosion of Materials, 2026 **Abstract:** High-temperature oxidation analysis is critical for the application of high-entropy alloys (HEAs) in aggressive environments. This review systematically assesses the oxidation behaviour of CoCrFeMnNi- and AlCoCrFeNi-based HEAs by evaluating the effect of alloy composition, temperature, oxygen partial pressure, alloying additions, phase constitution, microstructure, processing, and heat treatment on oxidation kinetics and oxide-scale evolution. Literature-reported parabolic oxidation rate constants are compiled and compared to elucidate mechanistic trends across different compositions. The CoCrFeMnNi-based HEAs generally exhibit inferior oxidation resistance because fast-growing Mn-rich oxides hinder the formation of a continuous protective Cr_2O_3 scale, whereas AlCoCrFeNi-based HEAs achieve significantly lower oxidation rates through the formation of slow-growing, thermodynamically stable α-Al_2O_3 scale. The review further demonstrates that oxidation performance is governed by the combined effects of elemental activities, phase constitution, microstructure, and oxidation environment rather than by the concentration of a single alloying element. Based on these mechanistic insights, design strategies are proposed to optimise alloy chemistry, phase constitution, microstructure, and processing to promote the formation of stable protective oxide scales for high-temperature applications.
58.	Hybrid model-based nonlinear economic model predictive control for energy optimization in a plug-in parallel hybrid electric agricultural tractor **VS Ghorpade**, BV Patil, **J Valluru** - Journal of the Franklin Institute, 2026 **Abstract:** Energy management in plug-in parallel hybrid electric vehicles for agricultural operations is a complex nonlinear constrained optimal control problem due to terrain induced rolling-resistance variations alter the traction demand. Further, rolling resistance coefficient (RRC) is difficult to measure in real time. This paper proposes a hybrid model based nonlinear economic model predictive control (EMPC) framework for optimal energy management of a plug-in parallel hybrid agricultural tractor under time varying unmeasured rolling resistance scenarios. The proposed strategy combines first principles dynamic models of vehicle, engine and battery dynamics, with linear and non-linear auto-regressive data driven residual models. Here, residual models capture time varying model plant mismatch within EMPC framework. In addition to tracking reference vehicle speed, the proposed EMPC directly minimizes brake specific fuel consumption (BSFC) based economic loss function, while satisfying state and actuator constraints. Simulation studies under representative rolling-resistance scenarios show that the proposed hybrid model based EMPC framework preserves satisfactory speed-tracking performance and reduces

	total energy consumption by 5.1–14.3% compared to the conventional hybrid MPC. These results demonstrate that hybrid model based EMPC is a promising real-time energy-management solution for agricultural hybrid vehicles operating under uncertain resistive loads.
59.	Impacts of sand mining on hydrochemistry and human health risk profile of Yamuna River water at Etawah, Uttar Pradesh **A Gani, S Pathak** - Environmental Research, 2026 **Abstract:** Yamuna is one of the main tributaries of the river Ganges which provides water to millions of people for drinking, agriculture and their livelihoods. In recent years, extraction of sand from the Yamuna River has increased significantly, which changes the river's physiological balance and leads to serious health risks. Sand mining may contribute to the mobilization of sediment-bound pollutants through sediment disturbances and resuspension processes. The present study assessed the impact of sand mining on the Yamuna River water quality at Etawah, Uttar Pradesh and assesses associated human health risks. Data pertaining to numerous physio-chemical and biological parameters was collected from the Central Water Commission (CWC) over a 25-year period spanning from year 1997 to 2022. The present study uses an integrated weighted water quality index (IWQI) and principal component analysis (PCA) based hybrid WQI. Human health risk for different demographic groups was assessed by using the US Environmental Protection Agency (USEPA) model, considering both carcinogenic and non-carcinogenic risk via ingestion and dermal exposure. Findings of the study demonstrated that high concentrations of turbidity, Biochemical oxygen demand (BOD), total coliform (Tcol) and ammoniacal nitrogen (NH_3). The integrated WQI varied from 137 to 2795.81, classifying water quality from poor to extremely poor quality, while PCA based WQI ranges from 5.67 to 31.71, which classified water quality from poor to very poor quality. Findings of human health risk assessment revealed that high value of hazard quotients particularly for infants and children for nitrite (NO_2), nitrate (NO_3) and fluoride (F) posing potential health risk of methemoglobinemia and fluorosis. Sensitivity analysis identified Tcol, turbidity, BOD and NH_3 as the significant parameters for water quality degradation. Results of the long-term assessment highlight that the sand mining activities significantly change the physio-chemical parameters of the Yamuna River which raises concerns about the health risk.
60.	Incomplete fusion in $^{193}Ir(^{12}C, x)^{205}Bi$ reaction at $E_{lab} \approx 5$-7 AMeV **Amanjot, Priyanka, S Kumar, R Kaur, M Kaushik**, MK Sharma, Y Jangid, **PP Singh** - Journal of Physics G: Nuclear and Particle Physics, 2026 **Abstract:** Low-energy heavy-ion induced reactions often involve incomplete fusion, but the dependence of incomplete fusion on various entrance-channel parameters remains unclear. In this work, we measure channel-by-channel production cross-sections of different evaporation residues populated via complete and/or incomplete fusion in $^{12}C+^{193}Ir$ system at $E_{lab} \approx$ 64-84 MeV (≈ 5-7 AMeV) using the stacked-foil activation technique followed by offline γ-spectroscopy. Experimentally measured excitation functions have been analyzed in the framework of the statistical model code PACE4 using different values of the level-density parameter (a = A/9-A/13 MeV^{-1}). In the analysis of excitation functions, the xn and pxn channels (after correcting with their precursor contributions) have been explained fairly well with a = A/13 MeV^{-1} ; however, almost all α-emitting channels showed substantial enhancement over PACE4 predictions, which has been interpreted as an inferred incomplete fusion contribution. The incomplete fusion fraction (F_{ICF}) increases overall from 12% to 18% over the studied energy range (64-84 MeV). For better insights into the onset and strength of incomplete fusion, the variations of F_{ICF} have been studied as a function of different entrance-channel parameters, which are found to increase with mass asymmetry, Coulomb factor, and neutron skin thickness. Further analysis suggests that the sharp-cut-off model, in which incomplete fusion is confined to $\ell > \ell_{crit}$, does not fully hold for this

	system, with the incomplete fusion strength consistent with contributions from $\ell < \ell_{crit}$. Projectile breakup-driven incomplete fusion is found to suppress complete fusion by ≈ 12% and ≈ 6% w.r.t. the universal fusion function and the improved fusion function, respectively. These findings highlight the critical role of projectile structure at 5-7 AMeV energies, with implications for high-spin spectroscopy and reaction modeling.
61.	Influence of heating pulse duration on high-harmonic generation from bulk, nanopowder, and composite boron nitride laser-induced plasmas **SR Konda, S Kumari**, P Barik…RA Ganeev - Optics & Laser Technology, 2026 **Abstract:** We present a complete investigation of high-order harmonic generation (HHG) from laser-induced plasmas (LIPs) formed on boron nitride (BN) targets with three different morphologies: bulk BN, BN nanopowder tablets (~165 nm particle size), and BN nanopowder embedded within a polymeric glue matrix. We have produced LIPs using heating pulses (HP) with nanosecond (ns), picosecond (ps), and femtosecond (fs) durations, while harmonic emission was driven by intense fs driving pulses (DP). We investigated the HHG as a function of LIP parameters, including DP energy, HP duration, and the temporal delay between ns-HP and fs-HP. Under fs ablation conditions, the composite made of BN nanopowder and epoxy glue produced the highest HHG efficiency, while bulk BN showed an enhancement in conversion efficiency when ablated with ps-HPs. The variation in HHG emission across various samples indicates a correlation between LIP formation, harmonic yield, and harmonic cut-off energy. Our experimental findings show a prominent role of target morphology and ablation method in optimizing plasma-based HHG from wide-bandgap materials.
62.	Integrating Gaussian random functions with genetic algorithms for the optimization of functionally graded lattice structures **P Agrawal, M Agrawal** - European Journal of Mechanics-A/Solids, 2026 **Abstract:** The properties of lattice-based structures can be enhanced by varying their geometric parameters in a graded manner, and the gradation can be tailored to extremize a particular objective. In this manuscript, we propose a non-gradient-based optimization framework to find the tailor-made graded profiles for lattice-based structures. The key challenge addressed in the work is to ensure the graded nature/smoothness of the underlying structure in a non-gradient-based optimization scheme. As we demonstrate in the manuscript, the conventional implementation of the genetic algorithm provides structures with abrupt changes, leading to issues such as stress concentration. In this work, we propose a Gaussian random function (GRF)/Gaussian process regression (GPR) integrated genetic algorithm to obtain an optimal graded lattice profile for a given objective. The integration of the GRF/GPR along with a projection operator ensures the smoothness of the designs at each stage of the optimization. We present several numerical examples to demonstrate that the proposed framework provides smoother designs that are less susceptible to stress concentration, while ensuring satisfaction of the underlying objective.
63.	Interactive simulation framework for Berry-phase and quantum transport phenomena in topological materials PK Sarswat, RS Singh, ML Free, G Kumar - Inventions, 2026 **Abstract:** The Berry phase plays a central role in modern electronics and acts as a foundation for a wide range of phenomena, from the anomalous Hall effect to topological insulators and valleytronics. However, in conventional analytical treatments, its geometric origin frequently stays abstract and unreachable. A thorough paradigm for computational visualization that clarifies the emergence and implications of the Berry phase in quantum electronic systems is presented in this paper. The simulation begins with a spin-½ model in a rotating magnetic field and uses real-time

	spin precession and field rotation tracking to demonstrate geometric phase accumulation on the Bloch sphere. Key ideas for comprehending tunable topological devices are revealed by the dynamic redistribution of Berry curvature and associated Berry-flux evolution when the framework is further extended to time-dependent Hamiltonians that reflect oscillating fields or shifting mass terms. Users can see local spin textures and phase progression within the Brillouin zone by mapping each k-point in momentum-space modules to a small Bloch sphere. Topology is linked to quantifiable device phenomena by a hybrid real- and momentum-space animation that links geometric phase evolution with observable transport behavior such as quantized Hall responses and Landau orbits. Together, these interconnected modules provide an interactive framework for exploring Berry-phase-related geometric and transport phenomena across complementary quantum-mechanical representations. Finally, these visualizations form an interactive and pedagogically rich toolset that unites geometric quantum theory with practical implications for next-generation electronic and spintronic devices.
64.	Interfacial modification of nanostructured GLAD TiO2 ETLs via KCl treatment for CsPbBr3 perovskite solar cells N Chandrakar…**M Kumar**, DP Singh - Materials Science in Semiconductor Processing, 2027 **Abstract:** All-inorganic, wide-bandgap (2.3 eV) $CsPbBr_3$ perovskite solar cells (PSCs) have garnered significant interest in stable photovoltaic applications owing to their excellent thermal and moisture stability. However, defect-mediated recombination and inefficient carrier extraction at the buried electron transport layer (ETL)/perovskite interface remain key factors limiting their photovoltaic performance. In this work, nanostructured TiO_2 ETLs were fabricated via glancing-angle deposition (GLAD) and subsequently modified with KCl to tailor the buried interface. The porous GLAD-TiO_2 structure influences the formation of the $CsPbBr_3$ layer. KCl treatment modifies the TiO_2 surface, reducing electronically active trap states and facilitating charge transfer at the TiO_2/$CsPbBr_3$ interface. X-ray photoelectron spectroscopy (XPS) and ultraviolet photoelectron spectroscopy (UPS) confirm the changes in the chemical and electronic properties of the TiO_2 surface after KCl treatment. The modified TiO_2 surface also promotes more uniform growth of the $CsPbBr_3$ layer. The PSCs incorporating KCl-treated GLAD TiO_2 ETLs exhibit a power conversion efficiency of 9.04% and an open-circuit voltage (V_{OC}) of 1.50 V, compared to the pristine TiO_2 ETL PSCs. The KCl-treated devices also show improved stability under ambient conditions (25 °C, 45–55% relative humidity) and under inert N_2 atmosphere. These results demonstrate that combining morphology-controlled GLAD-TiO_2 with KCl-mediated interfacial modification is an effective approach for reducing interfacial defects, improving charge extraction, and enhancing the performance and stability of all-inorganic $CsPbBr_3$ PSCs. 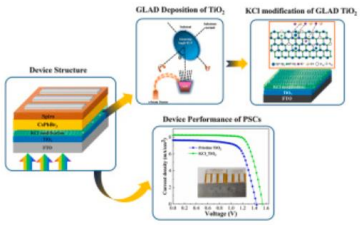
65.	Initial assessment of permeability and mechanical properties of NRL-treated recycled wool geomembranes **N Kumar, A Kumar, N James, M Raheena** - Proceedings of the Institution of Civil Engineers-Engineering Sustainability, 2026 **Abstract:** Geomembrane materials, predominantly composed of synthetic polymers, are extensively utilised as hydraulic barriers but pose ecological concerns. Although natural materials have been employed in a variety of geosynthetic applications, their use in geomembranes remains

	unexplored. This study explores the novel possibility of employing recycled wool fabric, surface-coated with natural rubber latex (NRL), as an environmentally friendly impermeable material for hydraulic constructions. The objective of the NRL coating was to improve the wool fabric's strength and impermeability. The wool fabric was treated by spraying it with NRL at different concentrations and immersing it in NRL. NRL treatment significantly enhanced the tensile properties of the fabric, increasing machine-direction strength by 225%–253%. Overall, the treated fabrics showed one to three times higher tensile strength in both machine and cross-machine directions than the untreated fabric. The fabric becomes impermeable after NRL treatment. The pullout and direct shear tests indicated that the untreated fabric exhibited higher interface friction and pullout resistance than the NRL-treated fabrics due to its rougher surface characteristics. Nevertheless, the interface properties of the treated fabrics remained within the desired range, demonstrating their suitability for geotechnical applications.
66.	Label-free analysis of grade-specific molecular alterations in osteoarthritic subchondral bone using Raman spectroscopy coupled with MCR-ALS **G Uppal, A Singh**, RN Parasuraman, A Kumar, **KC Jena, R Kumar** - Spectrochimica Acta Part A: Molecular and Biomolecular Spectroscopy, 2026 **Abstract**: Changes in subchondral bone metabolism are central to osteoarthritis (OA) progression, highlighting the need for sensitive, label-free analytical approaches capable of resolving molecular-level alterations in complex biological tissue matrices. Raman spectroscopy is a powerful, non-destructive tool for detecting molecular changes in intact pathological tissues; however, overlapping spectral bands obscure accurate interpretation. In this study, Raman spectroscopy combined with multivariate curve resolution–alternating least squares (MCR-ALS) was applied to human subchondral bone at different stages of osteoarthritic degeneration to identify grade-specific molecular changes. The MCR-ALS approach enabled decomposition of overlapping Raman spectra into distinct biochemical components attributed to mineral, lipid, and collagen. Comparative statistical analysis revealed grade-dependent biochemical alterations in osteoarthritic subchondral bone. No significant changes occurred in mineral or lipid content at the early stage; however, significant mineral reduction and enhanced lipid accumulation were observed in advanced-stage degeneration. Collagen content exhibited an initial increase in the early stage, followed by a substantial decline in the advanced stage, accompanied by progressive disruption of its structural organization. Deconvolution of the amide I band further enabled improved characterization of collagen structural changes in intact tissue. These findings demonstrate that the Raman–MCR approach effectively resolves complex biological spectra, sensitively detects stage-specific molecular alterations in osteoarthritic subchondral bone, and offers a robust analytical framework for the label-free characterization of intact tissues. 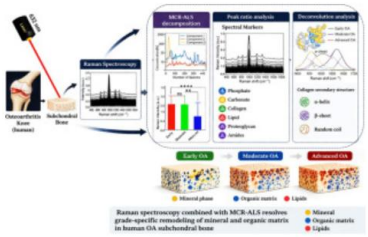
67.	Leveraging deep learning and kernel density representations for transformation-based regional flood frequency analysis **S Kaur, SR Chavan** - Journal of Hydrology, 2026 **Abstract:** This paper leverages deep learning (DL) and kernel density representations to determine design flood estimates at ungauged or sparsely gauged sites through transformation-based regional

	flood frequency analysis (T_RFFA) approach. A critical preliminary step in conventional RFFA approaches is to identify an appropriate regional frequency distribution through an effective regional goodness-of-fit (GOF) test. However, conventional regional GOF tests involve sample mean–based normalization of at-site peak flow data, which can violate key assumptions of RFFA. To address this, the proposed method reformulates regional GOF test as a classification problem wherein peak flow data from each site are transformed into a dimensionless space using mathematical transformations. Kernel density estimator (KDE) plots are then generated and used as inputs to a pre-trained Deep Neural Network (DNN) classifier that selects the most suitable regional distribution among the five widely recognized peak flow distributions, viz., Generalized Extreme Value, Generalized Pareto, Generalized Logistic, Generalized Normal, and Pearson Type 3 distributions. The DNN classifier achieved classification accuracies of 95.09% and 94.86% on training and test datasets, respectively. The effectiveness of the proposed DL-based RFFA approach is evaluated through Monte Carlo simulation experiments and real-world applications to catchments in the United States and peninsular India. Results demonstrate that the proposed approach yields comparable or better design flood estimates relative to conventional T_RFFA approach. Furthermore, the proposed DL-based GOF test is observed to be approximately 18 to 27 times faster than the conventional *L*-moment-based approach, offering a computationally efficient and robust alternative for RFFA.
68.	Leveraging iodomethylboronic ester reactivity to access late-stage dehydroalanine and dehydrovaline onto peptides in water **S Ghosh, S Chatterjee, A Bandyopadhyay** - Organic Letters, 2026 **Abstract:** We report a mild, chemoselective late-stage conversion of cysteine and penicillamine residues into dehydroalanine (Dha) and dehydrovaline (ΔVal), respectively, in peptides via rapid bis-alkylation with the commercially available iodomethylboronic acid pinacol ester (IMBpin) in PBS buffer. This operationally simple method affords largely excellent conversion to Dha/ΔVal containing peptide substrates. Such in situ generation of reactive alkene handles provides a powerful method for synthesizing post-translational mimetics, as demonstrated by the facile conjugation of thiol-bearing cargos (drugs, lipids, fluorophores, glutathione) under mild conditions in the same pot or with purified Dha-peptide, highlighting the method's potential in peptide engineering. 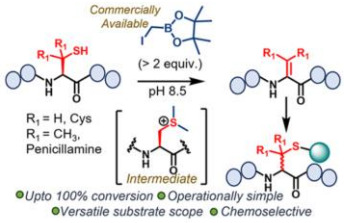
69.	Linking Synthesis-Structure-Performance for Low-Temperature CO2 Methanation over Pechini-Derived Ni/CeO2 Catalyst **AS Khan, T Mondal** - Catalysis Today, 2026 **Abstract:** Catalytic CO_2 methanation represents a promising route for carbon capture and utilization by converting CO_2 into synthetic methane compatible with existing natural gas infrastructure. In this study, 15 wt% Ni/CeO_2 catalysts were synthesized by four representative preparation methods, namely co-precipitation, wet impregnation, urea hydrolysis, and the Pechini sol-gel method, to systematically investigate the influence of synthesis strategy on catalyst physicochemical properties and CO_2 methanation performance. Comprehensive characterization using XRD, N_2 physisorption, H_2-TPR, CO_2-TPD, Raman spectroscopy, XPS, EPR, FESEM, HRTEM, and thermogravimetric analysis revealed that the Pechini-derived catalyst (NC-PSG)

	possessed a high surface area, improved Ni dispersion, enhanced metal-support interaction, abundant oxygen vacancies, and favorable reducibility compared with catalysts prepared by the other methods. Optimal performance was obtained at 325 °C, 5 bar, and GHSV of 17187 h^{-1}, where NC-PSG delivered a CO_2 conversion of 84 %, a CH_4 selectivity of 91 %, and a CH_4 yield of 77 %. The effects of reaction temperature, pressure, and gas hourly space velocity demonstrated that catalyst performance is governed by the combined influence of reaction kinetics, thermodynamic equilibrium, and residence time. A 100 h time-on-stream test confirmed stable catalytic performance under continuous operation. Post-reaction Raman spectroscopy, XPS, and thermogravimetric analyses indicated that the catalyst retained its structural integrity with negligible carbon deposition after prolonged reaction. Correlating the physicochemical properties with catalytic performance demonstrated that the superior activity and stability of NC-PSG originate from the synergistic effects of enhanced Ni dispersion, optimized metal-support interaction, abundant oxygen vacancies, improved reducibility, and suitable surface basicity. These findings provide a comprehensive structure–property–performance relationship for Ni/CeO_2 catalysts prepared by different synthesis routes and offer useful insights for the rational design of efficient catalysts for CO_2 methanation. 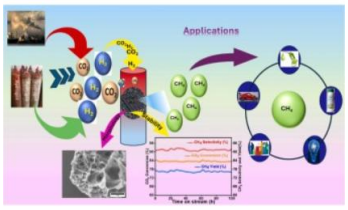
70.	Living drug carriers: Microbial and bioengineered platforms redefining precision therapeutic and immunomodulatory delivery L Guha, **JA Malik**, B Bose - Journal of Controlled Release, 2026 **Abstract:** Microbial living therapeutics are a new class of drug-delivery materials that combine synthetic biology, immunomodulation, and advanced formulations to achieve controllable therapeutic effects in space and time. In the broad field of living drug-delivery systems, therapeutic platforms include engineered microorganisms, mammalian immune cells, stem cells, viral vectors, extracellular-vesicle-producing cells, and hybrid bioengineered living materials. This review focuses on engineered microbial living drug carriers, including genetically modified bacteria and probiotic platforms, because these systems uniquely integrate programmable biosensing, in situ therapeutic synthesis, adaptive immunomodulation, and controllable drug delivery within a single living chassis. Designed microbes and consortia possess other unique functions, such as microenvironment sensing, programmed control of gene expression, and long-lasting in situ manufacturing of therapeutic payloads not available with small-molecule or biologic drugs. Recent progress in microbial chassis engineering, genetic circuit design, and biocontainment has enabled fine-tuning of immune responses, metabolic pathways, and tissue-specific signaling in a wide range of diseases from cancer to autoimmune and inflammatory diseases, to metabolic and endocrine disorders, neuro-immunological conditions (e.g., amyotrophic lateral sclerosis), infectious diseases including infectious threats without existing approved vaccines (Zika virus) as well as rare genetic disorders. Advances in formulation science, including encapsulation technologies, biomaterial-microbe hybrids, and stimuli-responsive release platforms, have enabled overcoming key translation challenges concerning microbial viability, biodistribution, safety, and controlled activation in complex physiological milieus like the gut (for enteric pathogens), tumor microenvironment (for oncolytic organisms), or injured tissues (for tissue-targeting organisms). Increasing numbers of clinical-stage LBP studies are now conducted under good manufacturing practice, standardized QC, and clinical conditions, ranging from emerging PK, biodistribution, and biomarker-driven studies to those adapted to living entities. The addition of host microbiome

	profiling, multi-omics analysis, and computational modeling is anticipated to increase therapeutic predictability and patient stratification. Taken together, these advances position live microbial therapeutics as programmable biological medicines with the potential for adaptive, context-specific administration and warrant further clinical development and increased integration within precision medicine–informed therapeutic approaches. 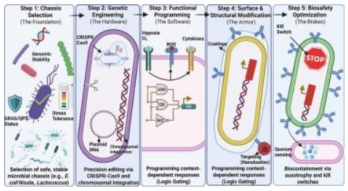
71.	Metal-dependent reaction pathways governing aromatic retention and deep hydrogenation in photocatalytic lignin hydrodeoxygenation **A Chauhan, R Ghalta, R Srivastava** - ACS Catalysis, 2026 **Abstract:** Selective control over reaction pathways in lignin hydrodeoxygenation (HDO) remains challenging under thermal conditions, where hydrogen activation and C–O bond cleavage are intrinsically coupled. Here, we demonstrate that visible-light photocatalysis enables control of the metal-programmed pathway by modulating hydrogen delivery via photogenerated charge carriers. Using Ru- and Pd-decorated sulfur-doped carbon/g-C_3N_4 heterostructures as common photoactive scaffolds, we show that metal identity governs hydrogenation depth under identical conditions. Ru selectively promotes ether C–O bond cleavage (β-O-4, α-O-4, 4-O-5) with aromatic product retention, whereas Pd drives cascade hydrogenolysis and deep ring hydrogenation to fully saturated hydrocarbons. This divergence extends from model substrates to native lignin. In situ UPS under illumination reveals quasi-Fermi level shifts and the formation of an interfacial chemical potential gradient ($\Delta\mu_{CN\rightarrow SCS} \approx 0.59$ eV), which drives directional electron transfer from g-C_3N_4 to the sulfur-doped carbon support and subsequently to the metal sites. Complementary REELS, kinetic isotope effects, and H_2–D_2 scrambling experiments are consistent with greater illumination-induced electron accumulation and hydrogen delivery at Pd than Ru. These findings demonstrate that photon-flux-controlled charge delivery modulates hydrogen availability at the metal sites, giving rise to distinct metal-dependent reaction pathways. This work provides a strategy for reprogramming biomass valorization pathways with a level of selectivity not accessible under conventional thermal conditions.
72.	Modeling the decay lifetimes of heavy and superheavy nuclei: A theoretical approach **R Kaur**, M Kaur, BB Singh, **PP Singh** - Nuclear Physics A, 2026 **Abstract:** In nuclear physics, the synthesis and measurement of decay lifetimes of heavy and superheavy elements (SHE) remains a central focus. The dominant decay pathways in this regime, α-decay and spontaneous fission (SF), serve as indispensable tools aimed at identifying new elements and are critical to understand their existence. Given the importance of these decay processes, we have systematically investigated how α-decay half-lives vary as a function of increasing neutron number (N; $N \geq 117$) in both heavy and superheavy nuclei. Since some α-decay chains culminate in nuclear fission, we also calculated the corresponding fission half-lives. Calculations are performed using the 'Preformed Cluster Decay Model' (PCM [T]), a method

	developed under the scope of quantum-mechanical fragmentation theory. This model incorporates temperature (T) dependence into the preformation and penetration probabilities of decaying fragments for an available set of experimental data. Furthermore, within this formalism, we estimates the α-decay half-lives of isotopes with atomic number Z=120. The results demonstrate that the PCM(T) is a robust model for reproducing the experimental half-lives of heavy and superheavy elements. Additionally, an analysis of the evolution of α-particle preformation probability (P_0) with increasing neutron number suggests the emergence of a possible sub-magic number effect at N=178.
73.	Multicomponent linkage engineering of quinoline-linked covalent organic frameworks for atmospheric-pressure metal-free CO_2 cycloaddition G Singh, **P Beniwal**, J Li, Z Jiang, T Liu, Y Gai, **TJ Dhilip Kumar**, X Feng - Small, 2026 **Abstract:** Developing efficient metal-free porous catalysts for the cycloaddition of CO_2 with epoxides under atmospheric-pressure conditions remains challenging because strong CO_2 affinity, efficient epoxide activation, and framework stability are difficult to integrate within a single material. Herein, we report a chemically robust bifunctional quinoline-linked covalent organic framework, Quinoline-COF_{COOH}, synthesized via a three-component Doebner multicomponent reaction. This approach enables the direct incorporation of CO_2-philic triazine units and Brønsted acidic carboxylic acid groups into an ordered porous framework without post-synthetic modification. Owing to the fused quinoline linkage, Quinoline-COF_{COOH} exhibits high crystallinity, permanent porosity, excellent chemical stability, and a surface area of 1296 m^2 g^{-1}. Compared with the imine-linked analogue, Quinoline-COF_{COOH} shows significantly enhanced CO_2 uptake and higher isosteric heat of adsorption (Qst = 43.2 kJ mol^{-1}), indicating strong framework-CO_2 interactions. Benefiting from the synergistic effect of triazine units and Brønsted acidic sites, Quinoline-COF_{COOH} efficiently catalyzes the cycloaddition of epoxides with CO_2 under atmospheric-pressure and metal/solvent-free conditions, achieving >99% conversion and selectivity within 6 h. Mechanistic studies and DFT calculations reveal that the carboxylic acid groups promote epoxide activation, while the triazine units facilitate CO_2 adsorption and insertion. This work highlights multicomponent linkage engineering for constructing a bifunctional COF for sustainable CO_2 conversion.
74.	Multigap superconductivity and pressure effects in the nontrivial superconductor **Reena**, C Li, **A Sharma**…**V Shukla** - Physical Review B, 2026 **Abstract:** Superconductivity (SC) remains a captivating field of research, promising transformative applications in energy, computing, and quantum technologies. Despite decades of investigation, the mechanisms underlying unconventional SC are not yet fully understood, motivating the discovery and study of new materials with exotic properties. The noncentrosymmetric superconductor PbTaSe2 offers a compelling platform to explore unconventional SC, where the absence of inversion symmetry can give rise to mixed-parity pairing states and novel superconducting phenomena. In this work, we investigate its superconducting properties through combination of specific-heat and muon spin relaxation (μ×SR) measurements, with the latter performed under both ambient and applied hydrostatic pressure. At ambient pressure, PbTaSe2 exhibits a superconducting transition at Tc=3.6K, with a normalized heat capacity jump Δ×C/γ×Tc=1.4, indicating weak electron-phonon coupling. A combined analysis of specific-heat and μ×SR data under ambient pressure reveals the presence of multigap s+s-wave superconductivity, characterized by two distinct superconducting gaps. Upon the application of hydrostatic pressure up to 3 kbar, Tc is significantly suppressed from 3.6 K to approximately 2.5 K, likely due to structural modifications involving the shift of the Pb atomic position without any change in the overall crystal symmetry. Notably, the multigap nature of the superconducting

	state persists under applied pressure. Furthermore, zero-field μ×SR measurements confirm the absence of spontaneous internal magnetic fields at ambient as well as applied pressure, demonstrating that time-reversal symmetry remains intact in the superconducting state despite the noncentrosymmetric crystal structure of PbTaSe2. Overall, these findings establish PbTaSe2 as a promising platform to study the unconventional SC and the interplay between multigap behavior, topology, and electron-phonon coupling under pressure. 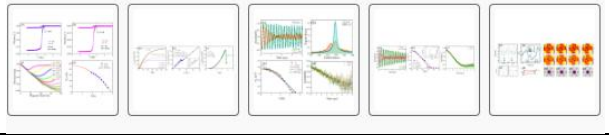
75.	Multiview ensemble deep generalized eigenvalue random vector functional link **Y Kumar, A Bhatia, C Jayrajsinh, M Ganaie** - Computers and Electrical Engineering, 2026 **Abstract:** The Random Vector Functional Link (RVFL) framework provides a simple and effective classification solution using a single-layer feedforward structure with randomization. The ensemble and deep variants of RVFL utilize multiple layers to improve performance, whereas the generalized eigenvalue-based deep RVFL (edGERVFL) solves a generalized eigenvalue problem integrated with the deep RVFL architecture. Multiview learning methods use multiple data views for enhanced generalization, but existing deep RVFL-based models do not incorporate multiview information. We formulate a Multiview Ensemble Deep Generalized Eigenvalue RVFL (MV-edGERVFL) and its variants — Multiview Kernel edGERVFL, Multiview Improved edGERVFL, and Multiview Kernel Improved edGERVFL — to achieve improved classification performance with multiple views of complex and non-linear data. The proposed model integrates multiview feature extraction with a deep ensemble of randomized networks based on generalized eigenvalue-based classification. To enhance applicability, we introduce three specialized variants that address non-linearity and singularity while retaining a closed-form solution. Multiview Kernel edGERVFL performs kernel mapping for non-linear separability. The Multiview Improved edGERVFL reduces singularity issues in correlated or sparse data. The Multiview Kernel Improved edGERVFL handles non-linearity and singularity together for improved stability. Experiments on UCI and AWA datasets offer consistent improvements when multiple data views are available. 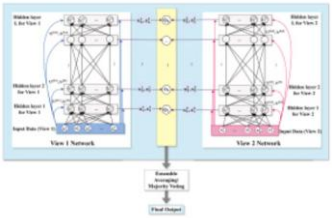
76.	On the behaviour of cycle integrals of jj invariant **B Kumar, J Kumari** - Mathematika, 2026 **Abstract:** In this paper, we study the values of modular functions at real quadratic irrationalities which are defined in terms of cycle integrals of modular functions associated with closed geodesics. We refine a result of Bengoechea and Imamoğlu to include values (and its limiting behaviour) of modular functions at a larger class of real quadratic irrationalities. As a consequence, we deduce the limiting behaviour of values of modular functions at powers of Pisot–Vijayaraghavan numbers. Further, we deduce distribution of class numbers of real quadratic fields having discriminants of a particular type.

77.	Pd-catalyzed chemodivergent monodefluorinative cascade cyclizations of gem-difluorovinyl-conjugated alkynylanilines to fluorinated benzocarbazoles and indoloisoquinolines **S Devi, M Kumar, D Kumar**, IS Koul, **A Goswami** - Organic Letters **Abstract:** An efficient one-pot Pd-catalyzed reaction medium-directed chemodivergent protocol has been developed that enables the controlled assembly of *meta*-fluorinated benzocarbazoles, fluoroindoloisoquinolines, and their halogenated analogues from easily synthesizable *gem*-difluorovinyl-conjugated alkynylanilines (*gem*-DFAA). The protocol exhibits a broad spectrum of substrate scope including late-stage coupling of fluorobenzocarbazoles with anti-inflammatory drugs and the synthesis of fluorinated analogues of inhibitors for estrogen receptors. 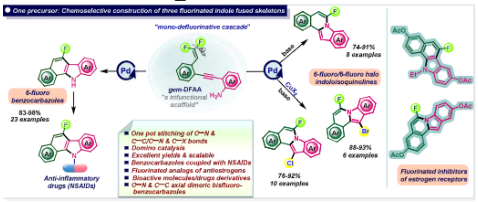
78.	Perception of instructors and students on kalarippayattu: a mixed-method study on an Indian martial art **AV Suresh, A Nandha** - Asian Journal of Sport History & Culture, 2026 **Abstract:** This paper aims to study the perception of kalarippayattu, an Indian martial art form, founded on the views expressed by instructors and students in the southern Indian state of Kerala. Speculated to have sustained through antiquity, the origins of this martial art form are shrouded in mythical tales. Despite its rich history, kalarippayattu has not gained its due academic interest from martial arts scholars. It is in this context that this study propounds a mixed-methods approach to analyse the contemporary perception of kalarippayattu among practitioners. The participants of the study include kalarippayattu instructors and students practising kalarippayattu. The study analysed participants' perception of changes in pedagogy and elicited supportive and critical observations on various aspects of kalarippayattu like health benefits, motivation of practice, challenges and suggestions for future growth. Correspondingly, the philosophy that dictates kalarippayattu is rooted in dharma, the Indian concept of ethics. Dharma in kalarippayattu extends beyond individual duties and responsibilities towards personal growth. The practitioner is trained to be committed to the larger society. The findings also highlight the positive perception of this martial art among its practitioners signifying the importance of the preservation and revival of kalarippayattu.
79.	Quantification of the creep, fatigue, and oxidation damage and life prediction **N Mehani, SC Roy** - International Journal of Damage Mechanics, 2026 **Abstract:** Materials at high temperatures may undergo damage due to the interaction of creep, fatigue, and oxidation. Since the last decade, many methods have been developed to predict the life of the materials under creep–fatigue interaction (CFI) loading. However, oxidation damage is very rarely considered in such prediction models. Moreover, most of the methods available in the literature use a lot of testing and data acquisition from pure fatigue, creep–fatigue, and pure creep tests. To overcome these difficulties, this article investigates the tensile hysteresis strain energy density method (THSED) available in the open literature. A modified THSED method that takes into account oxidation damage is proposed and implemented with four different materials for uniaxial CFI and hybrid CFI loading conditions. The proposed method could predict the CFI life of 304 SS, 304L SS, Mod. 9Cr-1Mo steel, and P92 steel within a scatter factor of ±2.0. The model parameter (γ), determined by the hit-and-trial method in the existing THSED method, is found to

	be dependent on the oxidation damage, strain rate, and hold time. The analytical expressions for the estimation of THSED for uniaxial and hybrid CFI loading conditions have also been derived.
80.	Quantum optical properties of solid-state defects using stage scanning confocal microscopy **N Singh, RV Nair** - Journal of Microscopy, 2026 **Abstract:** Solid-state quantum emitters (QEs) at room temperature are central to emerging technologies in quantum computing, communication, and sensing. These atomic-scale defects require high-resolution spatial and spectral characterisation to study their photophysical behaviour. To address this, we developed a stage-scanning confocal microscopy system optimised for nanoscale mapping and single photon level investigations of QEs in diverse host materials, fully automated and controlled via custom LabVIEW software. The system features high-precision three-axis translation stages with nanometre resolution, enabling accurate spatial scanning. A high numerical aperture (NA) objective lens ensures diffraction-limited optical resolution, while integrated photon-counting modules allow for sensitive detection of photoluminescence signals. The platform supports various spectroscopic measurements, including frequency-resolved and time-resolved photoluminescence. The system incorporates a Hanbury Brown and Twiss (HBT) interferometer for second-order temporal autocorrelation measurements to verify single photon emission. Designed for versatility, the system can accommodate a broad range of QE materials, including organic dye molecules, perovskites, and inorganic semiconductors. Furthermore, the setup enables the study of emission engineering through the manipulation of the local density of optical states, supported by the ability to collect large-scale statistical datasets. Overall, the flexibility and robustness of the platform make it ideal for quantum photonic, supporting fundamental studies and practical device development.
81.	Red emitting heteroleptic Ir(III)-complexes: Competent photocatalysts for chemoselective ring expansion of indoles K Agarwal, **D Dange**, L Devi, S Patil, T**JD Kumar**…- Chemical Communications, 2026 **Abstract:** 4-Quinolones and tryptanthrin are active pharmaceuticals, with great demand due to their biological activities. Phosphorescent Ir(iii)-dipyrrinato complexes are synthesized and employed as photocatalysts for one-step conversion of indoles to 4-quinolones and tryptanthrin, respectively, in high yields. The method is versatile; it utilizes just 1 mol% of Ir-catalyst under oxygen and blue light, much lower than the previously reported catalysts for quinolone synthesis. 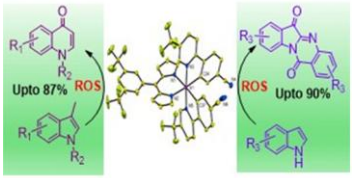
82.	Role of non-landslide data samples in improving landslide susceptibility mapping in the Western Ghats **S Kushwaha, N James**, B Pradhan, **SR Chavan** - Remote Sensing Applications: Society and Environment, 2026 **Abstract:** A reliable landslide susceptibility mapping (LSM) requires a comprehensive evaluation of the landslide inventory, predisposing factors, their interdependencies, machine learning algorithms, as well as the role of non-landslide data points, which, if poorly defined, can affect prediction accuracy. Despite advances in LSM, the systematic evaluation and impact of non-landslide data sampling (NLDS) strategies remain limited, leading to uncertainties in model reliability and spatial prediction accuracy. This study investigates the impact of certain NLDS strategies on improving LSM in the Idukki region of the Western Ghats (WG). We used a unified

	XGBoost framework integrated with SHAP analysis, providing statistical accuracy and spatial interpretability for a comprehensive and comparative assessment of LSM generated against each of the NLDS strategies (random, buffer-based, slope-based, modified information values (MIV)-based, and Mahalanobis distance (MD)-based). A total of 12 predisposing factors were used to generate 11 LSM scenarios across these sampling strategies. The results indicate that NLDS selection significantly affects both statistical accuracy and spatial realism. While the MD-based method performed best in terms of accuracy (0.9649; AUC: 0.9974), but over-predicted susceptibility zones. Buffer-based technique with buffer sizes of 1000 m to 2000 m provided well-balanced predictions (Accuracy: 0.9297; AUC: 0.9842). Slope-based sampling was found to be threshold-dependent, while MIV sampling was highly polarized, and the random sampling method performed the worst. The LSM balance predictions against each NLDS strategy are based on a comprehensive assessment of statistical measures, susceptibility class distribution outcomes, and spatial plausibility, rather than just AUC. SHAP analysis revealed that elevation, slope, and distance to road were the key factors, while their importance varied across methods. Overall, the findings emphasize the critical role of NLDS selection in improving the reliability and accuracy of LSM in landslide-prone areas.
83.	Role of Phase transformation, residual stress relaxation, and tribolayer formation on wear behavior of additively manufactured Ti6Al4V alloy BP Mahto, TS Kumar, VC Dinkar, RK Rai, **R Kumar**, MK Mishra - Tribology Letters, 2026 **Abstract:** This study examines the influence of post-processing heat treatment on tribological behavior of additively manufactured Ti6Al4V alloy. The specifically designed treatment promotes partial decomposition of metastable martensitic α′ phase into refined α+β structure and transforms residual stresses from tensile to compressive. Pin-on-disc tests showed that the heat-treated sample (HT950-WQ-650) exhibited lower wear rate than the as-printed sample. XPS analysis identified titanium oxides on worn surfaces of both samples. However, HT950-WQ-650 developed additional Al_2O_3-enriched tribolayer attributed to microstructural evolution associated with α′ → α + β transformation. The stabilized tribolayer reduces direct metal-to-metal contact, abrasive grooving, debris generation, and delamination. Subsurface analysis further revealed thicker plastically deformed layer with cracking and fragmented debris in the as-printed sample, whereas HT950-WQ-650 exhibited thinner deformation layer and reduced subsurface damage. The findings indicate that abrasive wear, delamination, and tribolayer instability dominate wear response of the as-printed sample, while stable Al_2O_3-enriched tribolayer and reduced subsurface deformation contribute to improved wear resistance of HT950-WQ-650.
84.	Role of refractive index distribution in shaping multimode soliton dynamics in GRIN-MMFs LK Sharma, **V Pal** - EPJ Web of Conferences, 2026 **Abstract:** Multimode optical solitons exhibit peculiar properties and holds potential for a large number of applications, from the next generation of high power lasers to the new spatially multiplexed communications systems. In this work, we theoretically study the impact of core refractive index distribution in a multimode fiber on the spatiotemporal dynamics and peculiar properties of multimode (MM) solitons. The characteristic MM soliton energy increases as the index distribution parameter (α) deviates from its optimal value of 2.08. Additionally, one can induce the flow of energy in a direction opposite to the conventional MM soliton condensation process with suitable value of the index distribution parameter (α).
85.	Scalable methods for storing and retrieving wikipedia revision histories for large-scale analysis **A Verma**, S Setia, G Demartini - ACM Transactions on the Web, 2026

	Abstract: The history-based content of Wikipedia has long served as a valuable resource for a wide range of research efforts in Natural Language Processing (NLP). However, due to Wikipedia's dynamic and ever-evolving nature, conducting large-scale temporal analyses requires the efficient retrieval and processing of historical article versions. One of the major challenges in this domain arises from the lack of robust and scalable tools capable of managing the vast volume of revision data that Wikipedia provides. This limitation often acts as a significant bottleneck in both data management and downstream applications. In this work, we present a comprehensive analysis of online algorithms designed to enable efficient compression and retrieval of Wikipedia's revision history. Our methods are supported by theoretical guarantees, demonstrating their ability to achieve high compression rates while maintaining favorable time–space trade-offs. The analysis emphasizes the practicality and scalability of our approach, particularly in environments constrained by memory or processing time. To operationalize these theoretical findings, we develop and release WikECD (Wikipedia Efficient Compression and Decompression), an open-source Python library that implements our proposed algorithms for large-scale Wikipedia revision compression, retrieval, and analysis. Experimental evaluations on sampled Wikipedia articles show that the method can reduce dataset size to as little as 6% of its original volume, achieving up to 94% compression while preserving reconstructive accuracy. To the best of our knowledge, this work constitutes the first detailed and rigorous study to analyze and quantify the compression of Wikipedia's complete revision history dataset, paving the way for scalable and reproducible NLP research based on historical web data.
86.	Secrecy outage and capacity analysis for UAV-assisted IRS-aided G2G system N Goel, P Kumar, S Jain, M Tolani, SV Yadav, **S Darshi** - Scientific Reports, 2026 **Abstract:** The integration of intelligent reflecting surfaces (IRS) with unmanned aerial vehicle (UAV) is rapidly emerging as a groundbreaking approach to enhancing the performance of 5G and beyond (5G+) wireless networks. This paper considers UAV-assisted-IRS-aided ground-to-ground (G2G) communication (UA-IRS-G2G) for improving the reliability of ground users (GUs) in infrastructure-less scenarios. To develop the mathematical framework for UA-IRS-G2G system, a height-dependent Nakagami-*m* fading channel is assumed for the IRS-to-GU links, while a Rayleigh fading channel is adopted for the G2G links, accounting for the multipath effect between the GUs. For the same, the cumulative distribution function (CDF) of the end-to-end signal-to-noise ratio (SNR) for signals transmitted via UA-IRS is derived. Furthermore, the closed-form expressions of secrecy outage probability (SOP) and secrecy capacity are also derived for the considered scenario. Additionally, diversity order is employed to enhance the reliability of the received signal at the receiver node in the proposed scenario. At the end numerical simulations are conducted to validate the accuracy of these theoretical derivations. The performance of the proposed work is compared with the existing state-of-the-art method reported in[11]. The results demonstrate that the proposed approach achieves better performance than the existing method in[11].
87.	Sm2O3 effect on structural, optical and isothermal properties of borophosphate glasses for solid-state lighting applications S Kumar, D Kumar…**N Bansal**, S Punj, K Singh - Journal of Alloys and Compounds, 2026

	Abstract: The effect of Sm_2O_3on the structural, thermal, and optical properties $55P_2O_5 - 15B_2O_3 - 10Na_2O - (20 - x)Li_2O - (x)Sm_2O_3$(x = 0.0, 0.5, 1.0, and 1.5 mol%) of glass and glass-ceramics are investigated. Sm_2O_3enhanced the creation of bridging oxygens by converting the phosphate units from $P^0 \longrightarrow P^n$where n = 1, 2, and 3, along with a non-linear trend in the oxygen packing density and molar volume. The band gap increases from 3.79 to 3.96 eV as Sm_2O_3increases in as-prepared glasses. The emission spectra are in the blue-pink region for glasses and shift towards the pure blue region in glass-ceramics, particularly due to the evolution of $Na_2B_6O_{10}$phase. The decay lifetime of glasses is decreased from 4.72 to 1.01 ms with Sm_2O_3concentration. The CIE (x, y) coordinates of x=1.5 glass are (0.38, 0.24), which is a closer approximation to pure white light coordinates (0.33, 0.33) emission, while in glass-ceramics, CIE coordinates are (0.16, 0.07). The conversion of glass into glass-ceramics provides a better, variable, and sample-based approach to functionalizing these materials for solid-state lighting applications. 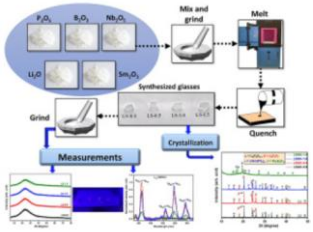
88.	Stereoselective gateway to decorated Chloro-1, 3-butadienes from Allenols via Deoxygenative 1, 2-bond migration **P Singh, AC Shaikh** - The Journal of Organic Chemistry **Abstract:** We disclose an efficient strategy for the selective synthesis of *E*-2-chloro-1,3-butadienes from allenols. This modular approach offers an extensive substrate scope with moderate-to-good yields and operational simplicity. Additionally, they offer a versatile platform for synthetic diversification and are highly scalable. 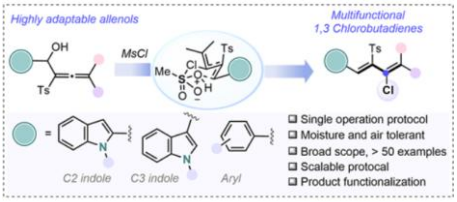
89.	Temperature shocks, renewable energy transition and inflation in island economies PK Narayan, K Rai, **B Garg**, V Vuniivi - Economic Analysis and Policy, 2026 **Abstract:** The objective of this paper is to explore the inflationary consequences of climate change and energy transition for Pacific Island Countries. Using appropriate econometric models, we show that temperature rises contributes to supply-side inflationary pressures, while output and demand-side factors appear to play a limited role. A one-standard-deviation increase in temperature affects inflation considerably, whereas renewable energy transition is associated with significant disinflationary effects. Oil prices and exchange rate depreciation further increase inflation through import-cost channels, while trade openness moderates price pressures. Mechanism tests indicate agriculture, labour-force participation, and energy demand as significant transmission channels. The findings highlight climate change as an important inflationary source and emphasize energy transition as a vital inflation-stabilisation policy instrument.

90.	Thermosolutal instabilities in inertialess thin self-rewetting liquid films on a vertical heated cylinder **M Zubair, R Vellingiri** - Physical Review Fluids, 2026 **Abstract:** We investigate the thermocapillary and solutocapillary instabilities in a self-rewetting liquid film that has a nonmonotonic variation of surface tension with temperature containing an insoluble surfactant at the interface. The dynamics of such a thin liquid film flowing axisymmetrically on a heated vertical cylinder is examined by deriving a set of coupled evolution equations for the film thickness and the surfactant concentration under the lubrication approximation. We perform a linear stability analysis of the steady film solution with a uniform surfactant concentration at the interface. The effects of solutocapillarity and quadratic thermocapillarity are analyzed in depth using Tm, the temperature at which surface tension is nearly minimum as the cutoff point, and $T0\times i,s$, the interface temperature of the steady film. Beyond a critical value of the solutal Marangoni number Mas, the dispersion curve, featuring two extrema exhibits midwave instability that is characterized by two cutoff wavenumbers. The conventional thermal Marangoni effect switches to the anomalous/reverse Marangoni effect as $T0\times i,s$ takes values greater than Tm. We perform a detailed parametric study to scrutinize the effect of thermal Marangoni number MaT, solutal Marangoni number Mas, Biot number Bi, Bond number Bo, and surface Péclet number Pes on the stability of the base state. The Orr-Sommerfeld problem is formulated and solved numerically under the creeping flow condition for arbitrary wavenumbers. A comparison of the neutral curves obtained from the Orr-Sommerfeld problem and the lubrication model reveal excellent agreement for small wavenumber perturbations. The nonlinear simulations of the coupled set of partial differential equations (PDEs) for the interface and surfactant concentration demonstrate the modulation of interface deformation in the presence of temperature gradients and concentration gradients in the regular Marangoni regime, whereas such deformations are suppressed in the anomalous Marangoni regime. 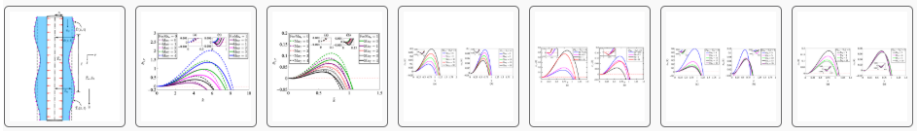
91.	Two-photon fluorescence and second-harmonic generation microscopy: Principles and biomedical applications KN Makkithaya…**R Kumar**, YV Kistenev… - Journal of Biophotonics, 2026 **Abstract:** Two-photon microscopy (TPM) has revolutionized biological imaging by enabling high-resolution, deep-tissue visualization with reduced photobleaching and photodamage. This review discusses complementary nonlinear optical imaging modalities such as two-photon fluorescence (TPF), second-harmonic generation (SHG), and fluorescence lifetime imaging (FLIM) microscopy that together provide structural, molecular, and metabolic information. The review begins by introducing the basic principles, instrumentation, and capabilities of two-photon fluorescence microscopy and FLIM. Followed by the development of SHG microscopy, highlighting advances from conventional SHG imaging to polarization-resolved, circular dichroism, and Stokes–Mueller polarimetric approaches. The biomedical applications of these complementary techniques are subsequently discussed, followed by an overview of multimodal imaging strategies that combine structural, molecular, and functional information. Collectively, these modalities represent a versatile and rapidly evolving imaging toolkit with broad potential to advance biomedical research, disease diagnosis, and precision medicine.

92.	Unravelling GLOF hazards in the Sikkim Himalaya: Simulating multi-lake flood scenarios under extreme conditions **VS Jadoun, D Gaikwad**, **RK Tiwari**, Abhishek - Earth Surface Processes and Landforms, 2026 **Abstract:** In recent decades, the Himalayan region has witnessed accelerated glacier retreat, driven by climate change, leading to the formation and expansion of glacial lakes. These lakes pose significant threats in the form of glacial lake outburst floods (GLOFs), which can be triggered by external events such as rockfalls, ice avalanches, intense precipitation and seismic activity. Previous Himalayan GLOF studies largely focused on single-lake breaches, whereas the cascading or simultaneous failure of multiple glacial lakes under regionally correlated triggers remains insufficiently explored. Given that many high-hazard lakes are located within similar hydro-climatic and seismic zones, understanding worst-case GLOF scenarios involving simultaneous breaches from multiple lakes requires detailed investigation. This study addresses this critical gap by rigorously quantifying the impacts of multi-lake GLOF events, considered among the most severe hazards threatening downstream communities. Using two-dimensional hydrodynamic modelling in HEC-RAS, we simulate the hydraulic behaviour of GLOFs originating from three highly vulnerable lakes: South Lhonak Lake, Gurudongmar Lake and Shako Cho Lake. The analysis encompasses seven distinct scenarios (S1–S7), ranging from individual lake outbursts to simultaneous breaches of all three lakes. Our findings reveal maximum flow depths ranging from 5 to 20 m, with flow velocities between 1 and 4 m/s. The worst-case scenario produced a peak discharge of approximately 9400 m^3/s at Chungthang, a critical downstream settlement. These findings highlight the potentially catastrophic consequences of multi-lake GLOF events, emphasizing the urgent need for integrated hazard assessment and proactive mitigation planning in vulnerable Himalayan river basins.
93.	Vacuum brazing of 3YSZ and CP-Ti using Ag-Cu-Pd filler alloy: Interfacial microstructure, phase evolution and hermeticity **A Upadhyay**, S Kumar, AK Singh, PD Kumar, **N Sardana** - Transactions of the Indian Ceramic Society, 2026 **Abstract:** Reliable and hermetic joining of ceramics to metals remains challenging due to interfacial incompatibility and thermo-mechanical mismatch effects. In this study, yttria-stabilized zirconia (3YSZ) was brazed to commercially pure (CP) titanium (Grade 2) using a nominally non-active Ag-Cu-Pd filler alloy (Palcusil), under high-vacuum conditions ($\sim 10^{-5}$/ mbar). The joint interface was systematically examined to determine the role of interfacial reactions in achieving effective bonding without active brazing elements. Scanning electron microscopy revealed a continuous, defect-free interface, while energy-dispersive spectroscopy confirmed redistribution of constituent elements across the joint. X-ray diffraction identified the formation of Ti_3O, $Ti_2Y_2O_7$, Cu_2TiO_3, Cu_3Ti_2, $Pd_{3.5}O_4$, along with Ag-rich and Cu-rich solid solutions, highlighting controlled phase evolution. Microhardness profiling showed the lowest hardness within the filler region relative to both parent materials, suggesting a compliant interlayer that may assist in accommodating processing-induced mismatch strains. Helium leak testing showed hermetic integrity with leak rates of the order of 10^{-9} $mbar.l.s^{-1}$, demonstrating suitability of the joints for vacuum-tight applications. The results demonstrate that the controlled interfacial phase formation enables the fabrication of hermetic 3YSZ-Ti joints using an active-element-free brazing alloy.

		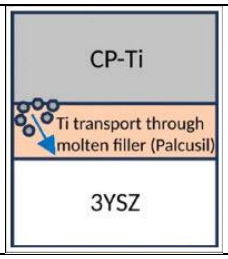
94.	Wave generation by initial impulsive disturbances in finite-depth water with an inertial surface **R Kumar**, **SC Martha**, BN Mandal - Physics of Fluids, 2026 **Abstract:** This paper investigates the two-dimensional Cauchy–Poisson problem in a finite-depth ocean covered by an inertial surface, involving impulsive initial disturbances. Three different types of impulsive disturbances, such as rectangular, Gaussian, and exponential profiles, are considered. Within the framework of linear water wave theory, the problem is formulated as an initial-value problem for the velocity potential describing the fluid motion. Laplace and Fourier transform techniques are employed to obtain the inertial surface elevation in an integral form. The resulting integral expression is analyzed asymptotically using the method of stationary phase for long time and large distance from the source of disturbance. The asymptotic behavior of the inertial surface is illustrated graphically for different values of the inertial parameter. The analysis of the three impulsive disturbance profiles reveals that increasing the inertial parameter reduces the wave amplitude, while waves associated with a higher inertial parameter persist for a longer duration and propagate over greater distances. Furthermore, the initial disturbance profile influences both the amplitude and phase of the waves generated by the different profiles. The rectangular and exponential profiles retain appreciable amplitudes over extended periods, whereas those generated by the Gaussian profile decay more rapidly and become negligible after a certain time. The results enhance our understanding of blast-induced wave generation and may aid in assessing their impact on ships, submarines, and coastal structures for naval defense and maritime safety.	

Disclaimer: This publication digest may not contain all the papers published. The library has compiled the publication data as per the alerts received from Scopus and Google Scholar for the affiliation “Indian Institute of Technology Ropar” for the month of September, 2026. The author(s) are requested to share their missing paper(s) details, if any, for the inclusion in the next publication digest.